2009-01-01

An Experimental Study Of The Hydrodynamics Of Multiphase Flow In Fluidized Beds

Gerardo Vargas
University of Texas at El Paso, gvargas2@miners.utep.edu

AN EXPERIMENTAL STUDY OF THE HYDRODYNAMICS OF MULTIPHASE FLOW IN FLUIDIZED BEDS

GERARDO VARGAS DUARTE

Department of Mechanical Engineering

APPROVED:

Ahsan R. Choudhuri Ph.D., Chair

Vinod Kumar, Ph.D.

Felicia Manciu, Ph.D.

Patricia D. Witherspoon, Ph.D.
Dean of the Graduate School

DEDICATION

This thesis is dedicated to the two women who supported me throughout my career, my mother, Yolanda Duarte, and my fiancée, Flor Ibarra.

AN EXPERIMENTAL STUDY OF THE HYDRODYNAMICS OF MUTLIPHASE FLOW IN FLUIDIZED BEDS

by

GERARDO VARGAS DUARTE, B.S.M.E.

THESIS

Presented to the Faculty of the Graduate School of

The University of Texas at El Paso

in Partial Fulfillment

of the Requirements

for the Degree of

MASTER OF SCIENCE

Department of Mechanical Engineering

THE UNIVERSITY OF TEXAS AT EL PASO

December 2009

Acknowledgements

Foremost, I want to acknowledge God and my parents for the overall education I was fortunate to have. I would also like to thank my Fiancée for her patience and support during my undergraduate and graduate degrees. It is also an honor to have worked under the supervision of my advisor Dr. Ahsan Choudhuri who helped me become a better engineering student.

It is a pleasure to thank my colleagues from the Combustion and Propulsion Research Laboratory who contributed in different ways in the development of my research. I would also like to show my gratitude to the members of my thesis committee, Dr. Vinod Kumar and Dr. Felicia Manciu, for their participation in the thesis revision and presentation. Last but not least, I would like to thank Ms. Elizabeth Gates for her contribution reviewing and formatting my thesis.

Abstract

Fluidized bed reactors have been widely used as a gasifier in coal gasification processes to convert coal into other forms of energy. At this stage, full fluidization is required to attain the best thermochemical reaction within the fluid-solid mixture. This can only be achieved if the fluid is maintained between minimum fluidization and terminal velocities. To better understand the hydrodynamics of multiphase flow, a fluidized bed was designed and constructed to carry out the investigation. Compressed air and 1-mm glass beads were used to determine gas minimum fluidization and terminal velocities at three different particle concentrations. The solids were enclosed in a 1.25-in inner diameter bed measuring 1 cm, 3 cm and 5 cm for each experimental setup. Additionally, pressure measurements at minimum fluidization were compared with theoretical values to corroborate the experimental results. In addition to gas flow rate measurements, the particles velocity at fluid terminal velocities was measured with two different techniques: laser doppler anemometer (LDA) and particle image velocimetry in Matlab (MatPIV) software. The first measured individual particle velocity in the axial direction, and the second measured the velocity of the particles as a whole. Lastly, video sequences of the fluidized bed are presented to provide a visual reference of the particles behavior at different fluidization stages.

Table of Contents

Nomenclature

U_{mf}	Minimum fluidization velocity
$\Delta_{\rho B}$	Pressure drop
Δp_{eq}	Buoyant weight per unit area of particles
g	Gravitational acceleration
M	Mass of particles
A	Cross sectional area of the bed
ρ_p	Particle density
ρ_g	Fluidizing gas density
μ	Dynamic viscosity
ε	Void fraction
f_p	Friction factor for a packed bed
L	Length of the bed
$Re_{\boldsymbol{p}}$	Reynolds number
U_s	Superficial velocity
Q	Volumetric flow rate

List of Tables

List of Figures

Chapter 1: INTRODUCTION

1.1 Overview

The current need to convert the energy content of coal into other forms of energy has been gaining a lot of interest among companies and citizens. Coal gasification is a process that is widely used mainly because of its high efficiencies and low emission of greenhouse gases. The process involves several stages of which the gasifier is the main component of the system. At this point, a fluidized bed reactor is used to carry out the different multiphase chemical reactions. Fluid and particle velocities are important in a fluidized bed reactor because at low flow rates the particles would be at a fixed state where low mixing occurs, as well as hot spots, within the bed that are not evenly distributed. Similarly, if excessive flow rate is input the solids are carried away from the gasifier. Gas-solid fluidized beds are used to simulate a fluid-like behavior within the gas-solid mixture, but it is complicated to understand the dynamic characteristics of the process due to the unpredicted behavior of the gas-solid flow. Nevertheless, pressure fluctuations, fluid and particle velocities can be used to define the dynamic characteristics of fluidized beds.

To obtain detailed information about gas-solid behavior experimental data are required. In this work, laser doppler anemometry (LDA), particle image velocimetry in Matlab (MatPIV) and pressure fluctuations are used to determine minimum fluidization and terminal velocities. Different particle concentrations are used in this investigation to simulate dense and diluted flows. Computer simulations are a powerful tool that is widely used because several codes have been developed to model gas-solid behavior in fluidized beds. Two methods can be used to pursue such study, Lagrangian and Eulerian. The first approach considers each particle separately, and the second analyzes all the particles as a continuum. In this work, the Eulerian approach is used because the solid and gas phases can be described together, which is the purpose of this research.

1.2 Research Objectives

The main objective of this study is to demonstrate how different particle concentrations affect the behavior of a fluidized bed. Determination of fluid minimum fluidization and terminal velocities are of great importance for this research. Moreover, a comparison between theoretical and experimental pressure values at minimum fluidization is also required to corroborate the results of the investigation. Lastly, particles velocities at fluid terminal velocity were measured and analyzed using the two different techniques.

1.3 Thesis Organization

Chapter 1 summarizes the importance of fluidized beds as well as their use in the alternative energy industry. Research objectives and facility information is also discussed in this section. Chapter 2 explains the fluidization behavior at different gas flow rates and provides detailed information about the stages of this process. Chapter 3 gives an outline of the design, construction and components of the experiment. This chapter also provides details about previous setup designs to observe how the experiment progressed from its initial approach. Chapter 4 explains the procedures that were used to measure pressure, particle and fluid velocities. The two different particle velocity measurement techniques are included in this section to understand their relevance to this research. Chapter 5 presents the results of the different phases of the experiment that were obtained with the data acquisition instruments, including discussions about the theoretical and experimental pressure values. Finally, Chapter 6 provides a conclusion about the experiment as well as recommendations for future research in fluidized beds.

1.4 Practical Relevance

Coal gasification processes depend on the gasifier to produce syngas and use it in the next stages of the system. If at this point in the process there is a poor thermo-chemical reaction, the entire gasification process is affected. For this reason, a good understanding of the hydrodynamics of fluidized beds is required to determine the fluid velocities where full fluidization occurs.

1.5 Combustion and Propulsion Research Laboratory

The investigation, including testing and analysis, was performed at the Combustion and Propulsion Research Laboratory (CPRL) located in the Mechanical Engineering Department at The University of Texas at El Paso. The facility is equipped with a wide range of instruments to perform experimental and computational research in the areas of energy systems, combustion and miniaturized space systems. These include the development of micro-propulsion and micro-combustion technologies.

Chapter 2: LITERATURE REVIEW

Detailed information about the importance of fluidized beds is presented in the following sections as well as the process involved in such systems to better understand the research covered in this paper.

2.1 Coal Gasification

The use of coal for energy purposes has been of a great concern for many years because of the pollution created in the process. Gasification is part of the clean coal technology that has been widely used for about 200 years because of its efficiency in converting solid coal into a cleaner gas fuel that can be easier to process [1]. Moreover, fluidized bed gasification is a well known technology that is used in electric power plants where coal is exposed to chemical reactions to produce syngas, which is mainly composed of hydrogen (H) and carbon monoxide (CO) [2]. The most important part of this process is the gasifier because the entire system depends on this. A fluidized bed reactor is used in this stage where the solid particles are exposed to a gas at predetermined flow rates to attain better chemical reactions, resulting from the efficient interaction of solids and gases.

2.2 Fluidized Bed

A fluidized bed is mainly a device in which solids and fluids interact with each other to create a fluid-like behavior that can be used for different purposes. For example, combustion processes, gasification of solid fuels or solid wastes, drying of particles, calcining, particle heating, regenerative heat exchangers, oxidation or reduction of ores, metal surface treatments and catalytic and thermal cracking [3]. Depending on the research, some setups use liquids or gases as a fluid for the solid-fluid mixture. The advantage of using liquids is that evaporation occurs in the interior of the fluidized bed, which allows cost savings for the evaporation in external heat exchangers [4]. Since the experiment designed for this investigation aims to contribute in future coal gasification research, the fluid used in the setup is compressed air.

There are several ways to put fluids in contact with solids within fluidized beds. Some of these methods include packed bed, flowing packed bed, spouted bed and falling cloud as shown in Figure 2.1.

In a packed bed, the containment vessel has a porous base known as the distributor where the particles rest and the fluid can be forced to flow upwards or downwards to provide fresh fluid continuously. This principle was used in this research with the fluid flowing upwards and with a slightly different design from the one shown in Figure 2.1.

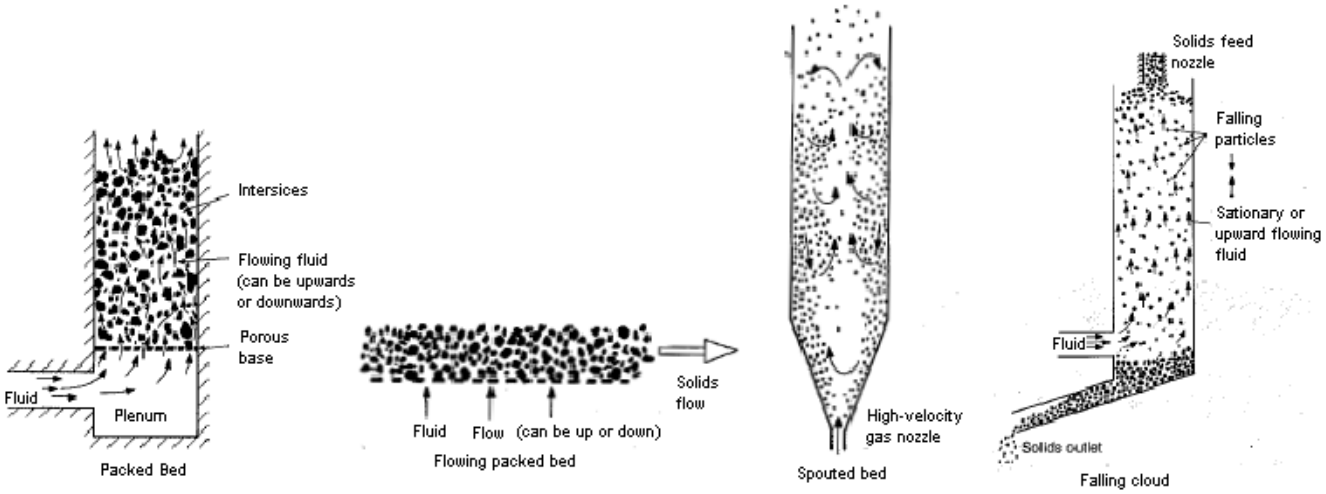

Figure 2.1: Alternative Gas-Solid Contacting Methods [3].

In a flowing packed bed, the bed is moving to create the interaction between solids and the fluid, which offers a good temperature distribution with the disadvantage that particle segregation may occur. Conversely, in a spouted bed there is a good agitation of particles due to the jet of fluid that passes through the bed at high velocities, but the high pressure drop at the beginning causes a problem in this system. Similarly, in the falling cloud methodology, the fluid is also forced upwards with the difference that the particles are being fed down from the top, offering a simpler setup that is dependent on reliable means of dispersing particles across the duct section [3]. Each method has its advantages and disadvantages and deciding which one is more suitable for each experiment depends on the researcher. The packed bed setup was chosen for this research because it offers a better resemblance to a gasifier used in coal gasification processes.

2.3 Fluidization

Fluidization as the name implies refers to a state where the solid-gas mixture presents a fluid like behavior. This occurs when the upward drag force in the particles, caused by the fluid injected from the bottom of the bed, equals the weight of the solids. Moreover, the obstruction to the flow, caused while the particles are at rest, causes a pressure drop that remains constant until the particles are in motion. Initially, this pressure drop $\Delta_{\rho B}$ will rise as the fluid velocity U is increased in a linear relationship as shown in Figure 2.2.

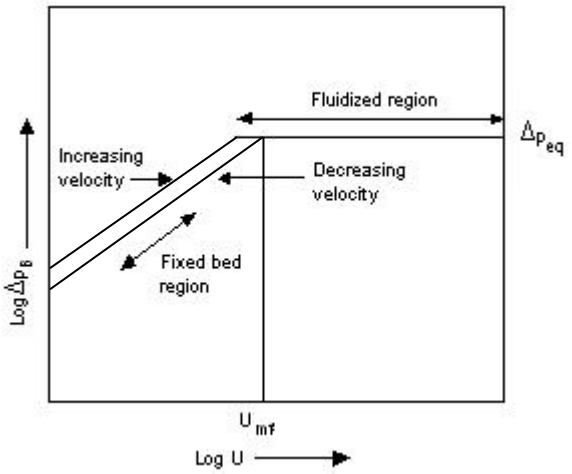

Figure 2.2: Ideal Pressure Drop-Velocity Curve [5].

When the velocity has reached such a value where the pressure drop is equal to buoyant weight per unit area of the particles (Δp_{eq}), minimum fluidization has been achieved. Any further increase in the velocity will not have any effect in the pressure drop because the particles will re-arrange so that the resistance to the flow is decreased [5]. However, there is a point in which the particles are carried away from the bed if the velocity keeps increasing after the terminal fluid velocity. Minimum fluidization and terminal velocities will be discussed later in this chapter (Sections 2.3.1 and 2.3.2). In addition, if the fluid velocity is now progressively reduced, there will also be a decrease in pressure drop, but the pressure drop-velocity curve will now be lower than the original because there is an absence of vibration as demonstrated in Figure 2.2.

The ideal pressure drop-velocity curve will never be attained because of some deviations that are caused by factors influencing the bed. For example, at minimum fluidizing velocity some bed expansion can occur before the pressure drop reaches a constant state. Furthermore, particles have a tendency to interlock with one another because of the frictional forces exerted by the walls of the bed; this can result in a higher value of pressure drop before the particles come apart showing a small "hump" as seen in Figure 2.3.

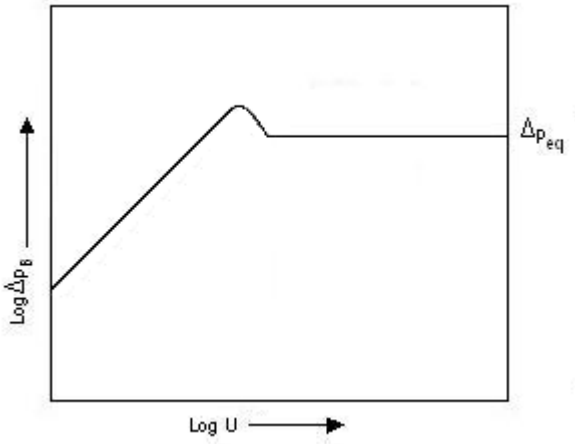

Figure 2.3: Effect of Particle Interlocking on Pressure Drop [5].

Once the bed is fluidized the pressure drop across it can be calculated as follows:

$$\boldsymbol{\Delta_{\rho B} = \frac{M}{\rho_p A}(\rho_p - \rho_g)g} \qquad \textbf{2.1}$$

Where M is the mass of particles, ρ_p is the particle density, ρ_g is the fluidizing gas density, A is the cross-sectional area of the bed containment, and g is the gravitational acceleration [3]. This formula applies in operations carried out at high static pressure, but most of the time the density of the fluidizing gas can be neglected [3] compared with that of the particles leading to:

$$\boldsymbol{\Delta_{\rho B} = \frac{Mg}{A}} \qquad \textbf{2.2}$$

2.3.1 Minimum Fluidization Velocity

Minimum fluidization velocity can be determined empirically from Figure 2.2 where pressure drop starts to remain unchanged, meaning it is equivalent to the weight of the bed. At this point, the bed presents a bubbling behavior, indicating that fluidization starts at this flow rate. This velocity can also be calculated as follows [6]:

$$\boldsymbol{U_{mf} = \frac{(\rho_p - \rho_g) g D_p^2 \varepsilon^3}{150 \mu\ (1-\varepsilon)}} \quad \textbf{2.3}$$

Where D_p is the equivalent spherical diameter of the particle defined by:

$$\boldsymbol{D_p = 6 \frac{Volume\ of\ the\ particle}{Surface\ area\ of\ the\ particle}} \quad \textbf{2.4}$$

μ is the dynamic viscosity of the fluid and ε is the void fraction of the bed, which corresponds to the ratio of the void volume to the total volume of the bed [6]. Equation 2.3 also called the Kozeny-Carman Equation applies only in a viscous flow regime for small particles ($D_p \leq 1mm$) and relatively small Reynolds number ($Re \leq 10$). For large particles ($D_p \geq 1mm$), the Ergun Equation should be used [6]:

$$\boldsymbol{f_p = \frac{150}{Re_p} + 1.75} \quad \textbf{2.5}$$

Where f_p and Re_p are defined as:

$$\boldsymbol{f_p = \frac{\Delta p\ D_p \varepsilon^3}{L \rho_g U_s^2 (1-\varepsilon)}} \quad \textbf{2.6}$$

$$\boldsymbol{Re_p = \frac{D_p U_s \rho_g}{(1-\varepsilon)\mu}} \quad \textbf{2.7}$$

In the above relations, L is the length of the bed, f_p is the friction factor for the packed bed, and U_s is the superficial velocity, which is calculated as:

$$\boldsymbol{U_s = \frac{Q}{A}} \quad \textbf{2.8}$$

where Q is the volumetric flow of the fluid. When the superficial velocity (U_s) equals minimum fluidization velocity (U_s), a state of incipient fluidization has been reached. Void fraction (ε) for the above relations will depend upon the material shape and size, but for nearly spherical particles a range from 0.40 to 0.45 can be used [7].

2.3.2 Terminal Velocity

Fluidization starts at minimum fluidization velocity. This stage is maintained at higher flow rates until a point is reached where the differential pressure is just higher than the weight of the bed, causing the particles to be carried away from the bed, as shown in Figures 2.4 and 2.5.

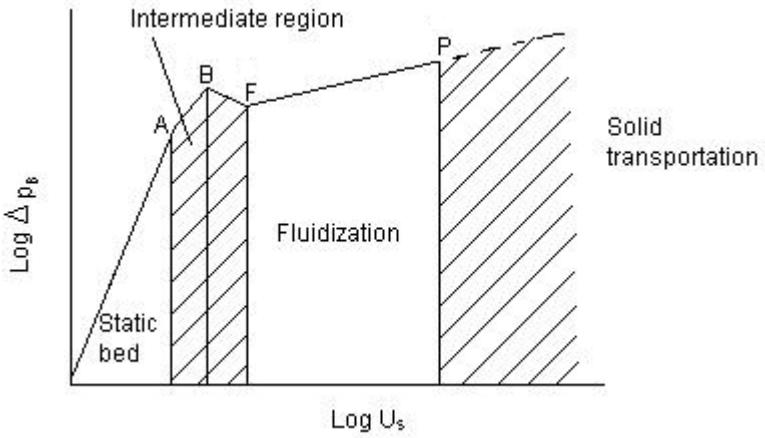

Figure 2.4: Pressure Drop in Fluidized Bed [8].

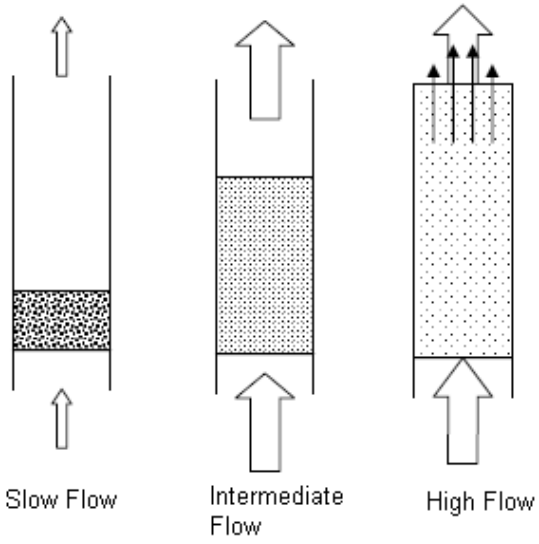

Figure 2.5: Fluidized Bed Stages at Different Flow Rates [9].

Figure 2.4 shows that initially the bed is at a packed or static bed state until the velocity reaches point *A.* At this point, the pressure drop equals the force of gravity and the particles start to lose contact with each other. At point *B,* the bed is extremely loose and with a further increase in the velocity the bed reaches minimum fluidization velocity at point *F* where true fluidization begins. After point *A,* there is an intermediate region where the particles adjust to present as little resistance to flow as possible until the grains separate to reach point *F*. As the superficial velocity keeps increasing, the bed continues to expand until the particles are entrained in the fluid at point *P* in which the fluid velocity is approximately equal to the terminal velocity [8]. What happens after the terminal velocity can be explained in terms of forces. Figure 2.6 shows how the buoyancy force and the fluid drag oppose the effect of gravity, and, when they are greater, the particle is carried away in the direction of the flow.

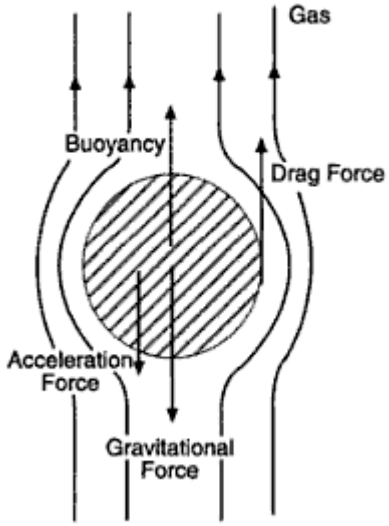

Figure 2.6: Force Balance on a Particle moving in an Upward Stream [10].

Figure 2.6 shows the schematic of a particle falling freely from rest, but if both the particle and gas move in an upward direction the particle will experience a fluid drag due to the relative velocity resisting its fall [10]. Therefore, the force balance under steady state becomes:

$$Gravitational\ force = Buoyancy\ force + Drag\ force \quad [10]$$

Chapter 3: EXPERIMENTAL SETUP

This chapter presents the system design and configuration along with the components of the fluidized bed experiment. Detailed information about the data acquisition equipment, which was used in the development of this research, is also included.

3.1 System Components

Figure 3.1 shows the schematic of the setup with the basic components and tubing dimensions. The fluidized bed was made of plexiglass tube with an outside diameter of 1.5 in and a wall thickness of 0.125 in. Moreover, the tubing was polyvinyl chloride (PVC) pipe Schedule 80 with an inside diameter of 0.526 in. All materials were securely glued with heavy duty PVC cement.

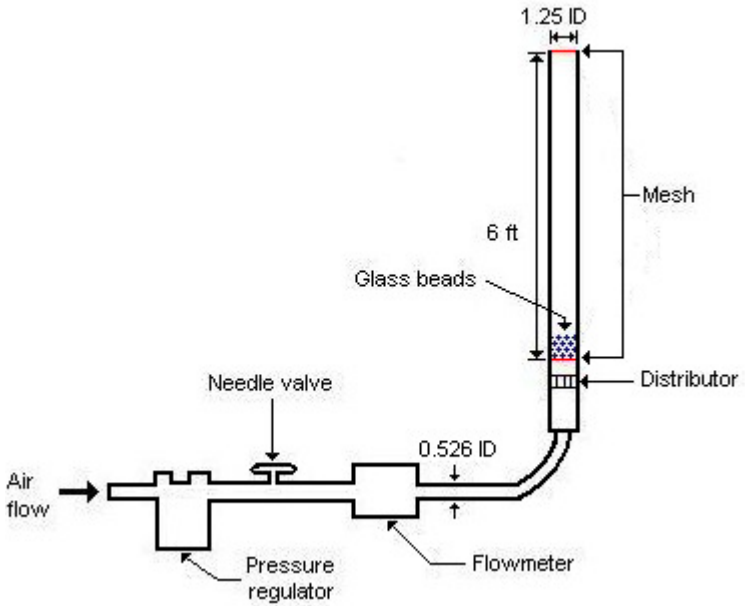

Figure 3.1: Fluidized Bed Schematic.

The solid particles used in the experiment were 1-mm glass beads with a density of 2.23 $\frac{g}{cm^3}$ and sphericity variation of $\pm 10\%$.

Since particle concentration was the main variable in the investigation, the weight had to be measured with a precision balance (Figure 3.1) prior the execution of the experiment.

Figure 3.2: OHAUS AV53 Adventurer Pro Precision Balance.

In order to ensure laminar flow, a distributor (Figure 3.3) made of copper tubes with a honeycomb shape was installed about 2.88 in above flow exit, which functioned as a flow straightener. Furthermore, in order to prevent the particles from falling back into the tubing and/or out of the bed, a mesh with a nominal diameter of 0.425 mm was installed at the top of the bed and about 1.88 in above the distributor.

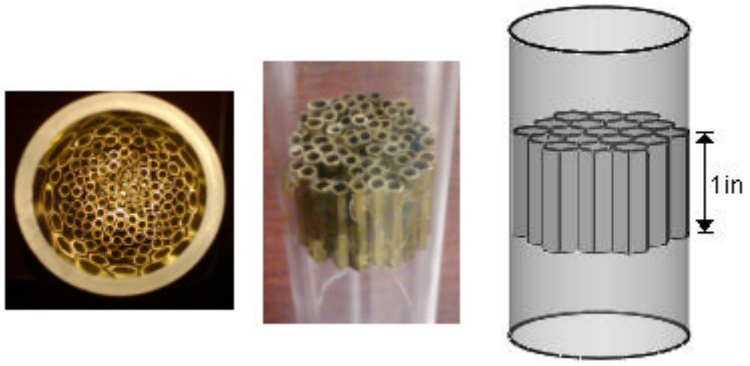

Figure 3.3: Distributor (Honeycomb Flow Straightener).

The experimental facility as illustrated in more detail in Figure 3.4 consisted of a (1) pressure regulator, (2) needle valve, (3) flowmeter, (4) distributor, and (5) additional ports for future experiments.

Figure 3.4: Fluidized Bed Experimental Facility.

3.2 Flow Control

The fluid used in the experiment was compressed air supplied by the compressor shown in Figure 3.5. The flow was controlled with a pressure regulator (Figure 3.6) and a stainless steel integral bonnet needle valve (Figure 3.7). Although the pressure regulator also offered the ability to filter and lubricate the air, only the air filter was employed. The pressure in the line was never higher than 50 psi because of the limitations of the PVC pipe transporting air. Lastly, the flow was measured with a digital mass flowmeter (Figure 3.8).

Figure 3.5: INGERSOLL-RA ND SSR-EP25 Air Compressor. Rotary Screw Horizontal Tank.

Figure 3.6: SMC AC40-N04C3-Z Air Filter, Pressure Regulator and Lubricator.

Figure 3.7: Swagelok SS-1RS8 Needle Valve for Precise Flow Control.

Figure 3.8: Omega FMA 1845 Digital Mass Flowmeter.

3.3 Data Acquisition Equipment and Procedure

Three different instruments along with data acquisition software were used in the development of the experiment. Figure 3.9 shows how the (1) differential pressure transducer, (2) high speed camera and (3) LDA were positioned to obtain the required measurements and test the bed under different circumstances.

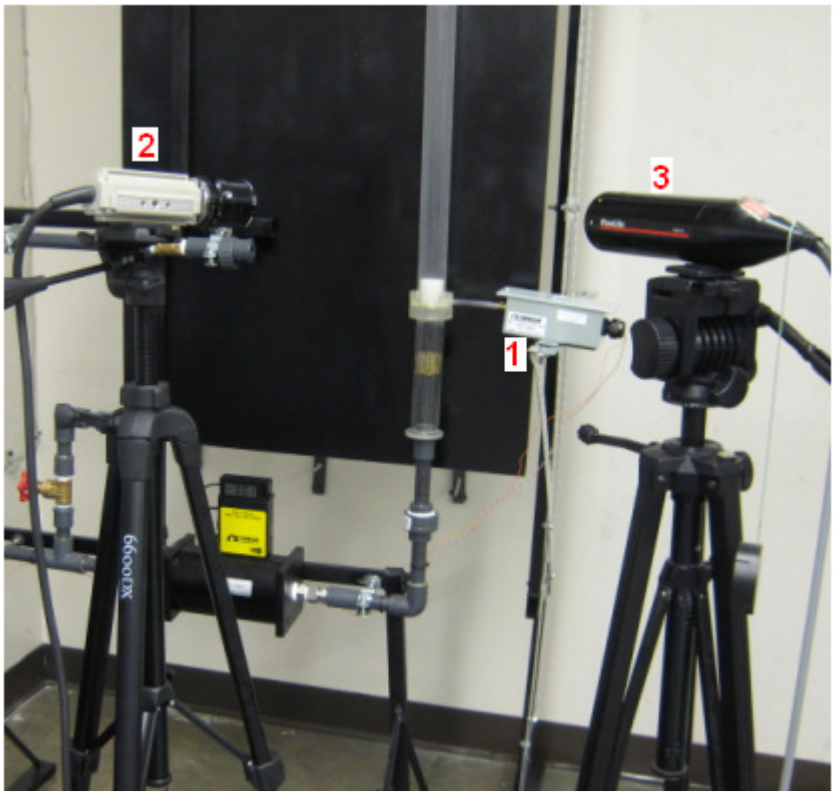

Figure 3.9: Schematic of Data Acquisition Devices.

3.3.1 Pressure Transducer

A differential pressure transducer (Figure 3.10) was installed at the bottom of the bed to help identify the flow rates where minimum fluidization and terminal velocities are present in the experiment. The device has six field selectable ranges, which send electrical signals as a function of the difference in pressure between the inside and outside of the bed. This differential pressure transducer was chosen over a regular gauge pressure sensor because of the possibility to select different pressure ranges.

The output configuration was set to be uni-directional with the maximum voltage range of 0 to 10 VDC to better identify the fluctuations in the 0 to 0.541 PSI input range. These ranges were selected after testing the bed at different conditions such as flow rates and particle concentration.

Figure 3.10: Omega PX277-30D5V Differential Pressure Transducer.

Multifunction Data Acquisition

The pressure transducer was connected to the terminal block shown in Figure 3.11 to measure the output voltage with a data acquisition (DAQ) device and send the signal to the computer software (Figure 3.12). Two 100 kΩ resistors were connected from the +/- pins to AI GND to reduce signal noise.

Figure 3.11: National Instruments Terminal Block NI SCC- 68.

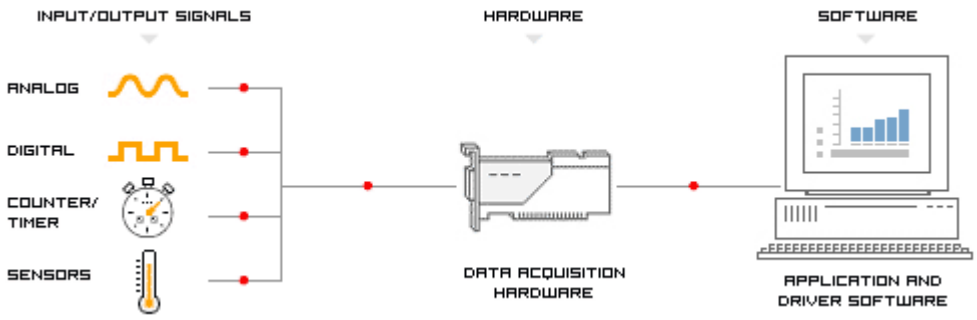

Figure 3.12: PC-Based Data Acquisition Schematic.

The system was powered by a linear DC power supply (Figure 3.13) set to 20 VDC as indicated in the pressure transducer input voltage requirements.

Figure 3.13: LOKO-Power Supply DPS-3050.

LabVIEW

LabVIEW version 8.2 is the computer software used to display and store the output signals from the pressure transducer. The front panel and block diagram from the virtual instrument (VI) file are shown in Figure 3.14.

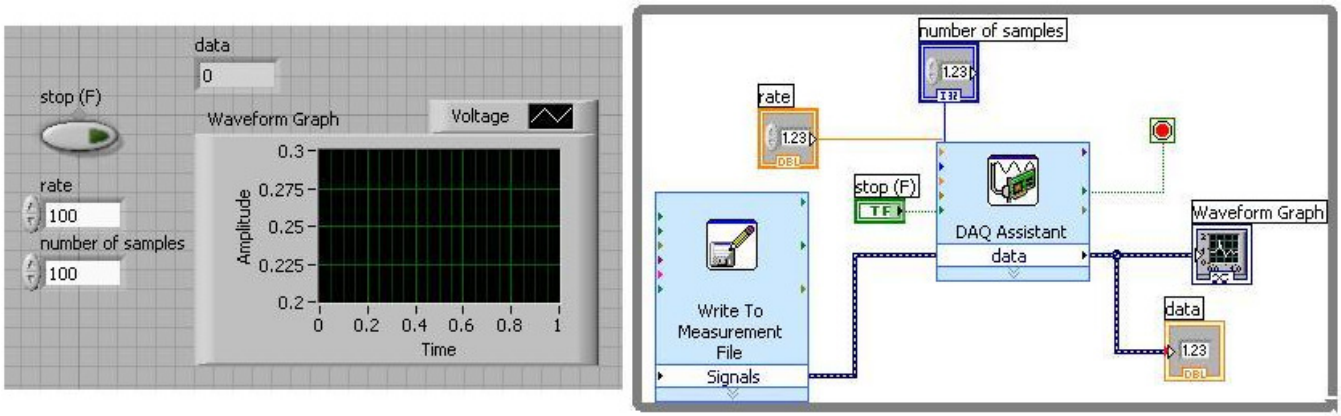

Figure 3.14: LabVIEW VI File with Front Panel and Block Diagram.

3.3.2 High Speed Camera

A high speed camera (Figure 3.15) system was used to record particle movement at the top the fluidized bed. This point occurs at the maximum height attained (in average) by the particles when lifted by the fluid. These measurements were taken at the flow rates where terminal velocity was detected with the differential pressure transducer.

Figure 3.15: PHOTRON FASTCAM-Super 10K High Speed Camera.

The recordings were later formatted in Vegas Pro 9 software (Professional HD video and audio production) to obtain consecutive images of the particle movement at different time intervals.

Lastly, these images were inputted into Matlab (MatPIV) to perform image processing and determine the particle velocity. (*The specifications for most of the components mentioned in this and previous sections are shown in the Appendix*).

MatPIV

MatPIV is a toolbox for PIV to run with MATLAB. This toolbox uses pattern matching techniques found in PIV fundamentals. The images have to be first formatted before being input into the software otherwise the particles would not be detected. The software creates and registers a pattern in the flow field of the particles in a 2-dimensional plane known as “light sheet.” The pattern is then used for pattern matching, which provides displacement information that if divided by the time separation between the two images gives particle velocity [11].

3.3.3 Laser Doppler Anemometer

Another velocity measuring technique is included in this research to better understand the hydrodynamics of a fluidized bed. LDA (Figure 3.16) is a non-intrusive and well-established technique for measuring local instantaneous velocities in single phase transparent flows [12]. The method may as well be used for multiphase measurement as long as optical access is possible and the system is diluted enough to allow transmission of the laser beam and scattered light [13].

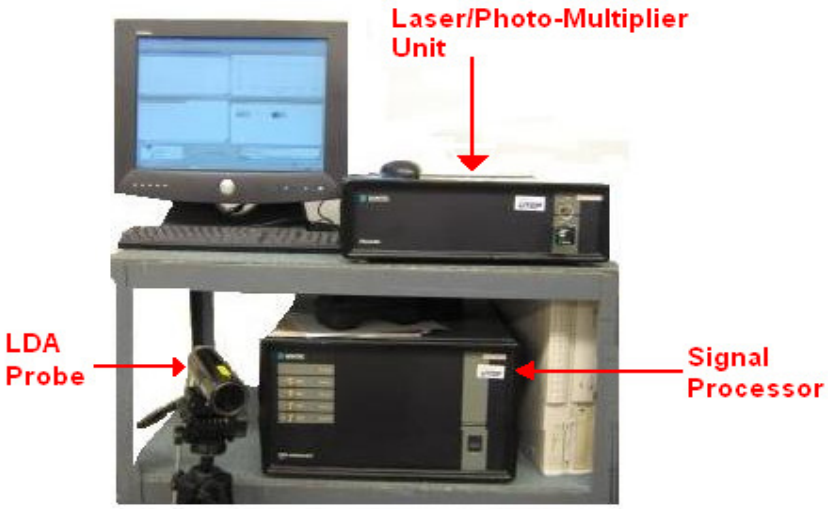

Figure 3.16: Dantec Dynamics LDA two Beam Red Wavelength System.

Depending on how the probe is positioned the LDA would allow for measuring the velocity of the particles in the axial and tangential directions. This is accomplished by turning the probe so that the laser beams are either vertical or horizontal. These intersecting beams create a fringe pattern (Figure 3.17) and as the particle passes through this point the light pulsates due to the reflection. The pulsating light is measured by a photodetector and the frequency along with the fringe spacing is used to compute the velocity [14]. Since the measurement surface has to be perpendicular to the laser beam only axial velocities were calculated for this investigation because the curvature of the plexiglass would cause refraction of the laser beam.

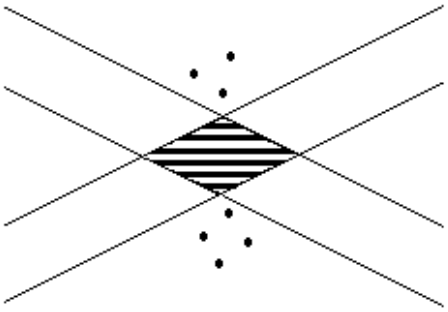

Figure 3.17: LDA Beams Fringe Pattern.

Although the results from MatPIV show the velocities of the particles as a whole in a determined section of the bed and the LDA measures the velocity of each particle that crosses the beams, the results can be compared if the LDA is positioned in different points of the target area. For example Figure 3.18 was taken from [11] where the magnitude of the velocity (b) was calculated from the movement of particles in water (a) with the MatPIV software. If, on the other hand, the velocity of the bottom section of the image (or any other section) was of interest, a point would be selected from (a) as shown in Figure 3.19. The laser probe would be positioned so it measures the velocity of the particles in the direction of the flow, and the results can be close enough to be compared with those from MatPIV. Moreover, if the measurement surface is flat the laser probe can be positioned at different angles to get the average velocity and direction of the flow. Depending on the objective of the investigation several measurement points can be used to observe the fluid behavior in a determined section of the experiment.

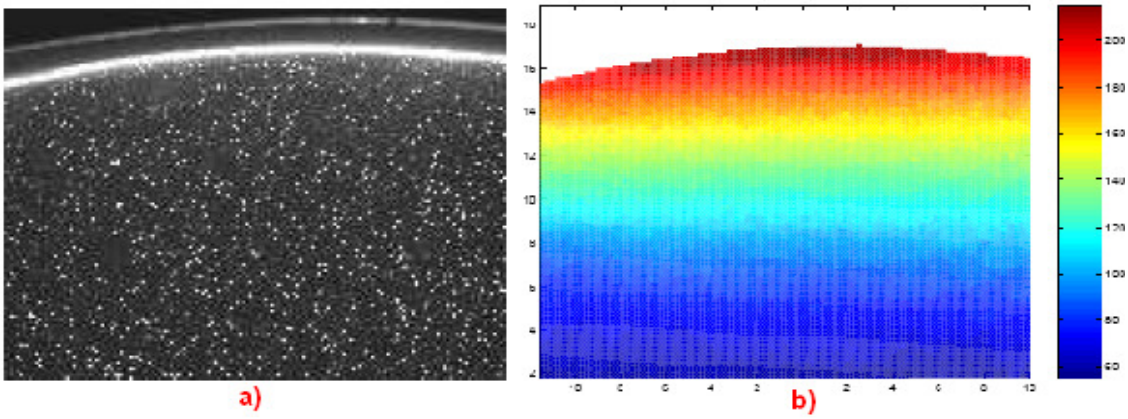

Figure 3.18: MatPIV Output Sample Images [11].

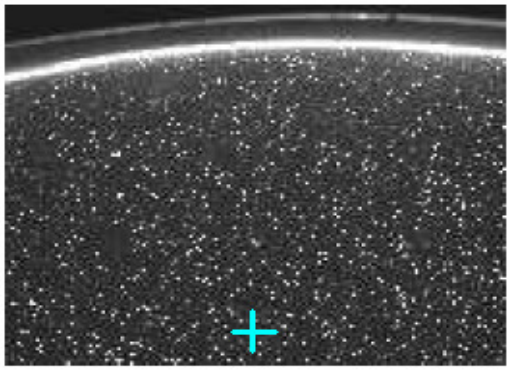

Figure 3.19: LDA Measuring Point.

FVA Software

FVA flow software was used in combination with the Dantec Measurement Technology to carry out the experiment. The package communicates with the hardware, acquisition of data or import of data, and statistical processing of data. The software "wizards" set up the processors, traverse and traverse mesh. Results can be presented in lists and histograms. The software is designed to run on a PC as an ordinary MS-Windows application. Windows 95 OSR 2(4.00.950.B) or later versions, or Windows NT 4.0 Service Pack or later versions is required. Figure 3.20 shows the user interface, which enables the user to control the set-up of all instrumentation in the LDA system, data acquisition as well as data analysis options, making LDA experiments straightforward and flexible [15].

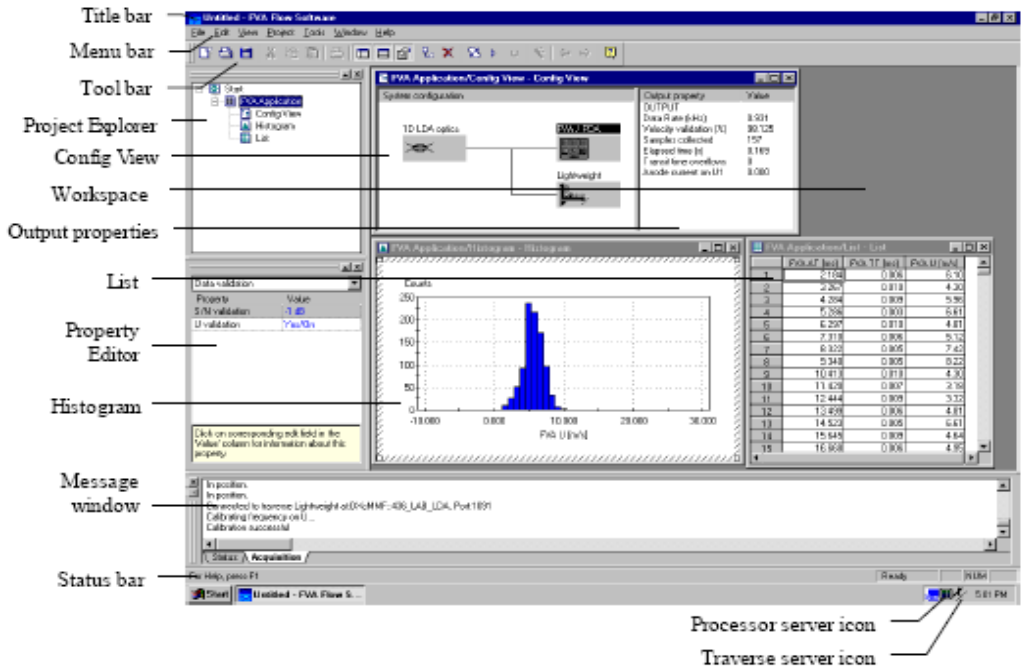

Figure 3.20: FVA Software User Interface.

3.2 Previous Designs

Several models were designed and/or constructed before the final setup was built. Figure 3.21 shows the first model with a different distributor design as well as different components. The system consisted of a (1) humidifier to get rid of static in the particles, (2) mass flowmeter(s), (3) pressure regulator and (4) cyclone. The model was discarded because of practical reasons including material availability.

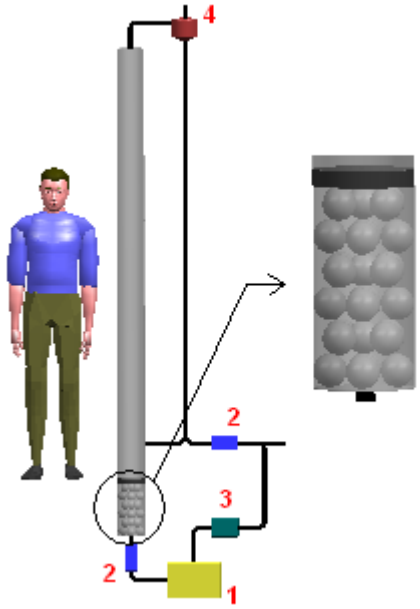

Figure 3.21: First Fluidized Bed Design.

A second system was actually built that was similar to the existing setup but the difference was that it had a shorter bed and a cyclone (Figure 3.22) to have a circulating fluidized bed. As the name implies the purpose was to have the particles circulating across the bed, however, it was discovered that the flow was being altered by recirculating the gas-solid mixture from the side of the bed and as a result the model was also abandoned.

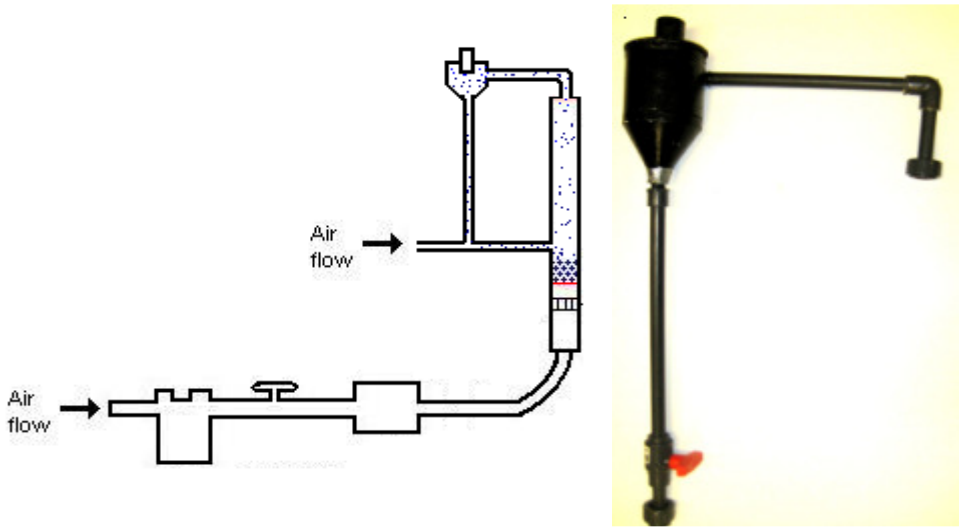

Figure 3.22: Cyclone Included in Previous Designs.

The final modification to the last model was the length of the bed. The system had a 3-ft long bed, but the height was not long enough to attain full fluidization because the particles were blocking the exit at very low flow rates, causing a significant increase in pressure. A 6-ft long bed was later installed leading to the final experimental setup shown in Figure 3.3. Lastly, since the humidifier from Figure 3.21 was not included in the final design a commercial anti-static spray was applied to the particles before executing the experiment.

Chapter 4: METHODOLOGY

Three different particle concentrations were used in the experiments to observe the transition from dilute to dense flow in a fluidized bed. Each concentration of particles measured 1 cm, 3 cm, and 5 cm weighing approximately 11.09 g, 33.28 g and 55.46 g, respectively. With the given particle specifications the 1-cm, 3-cm and 5-cm bed contained approximately $28.2X10^9$, $47.4X10^9$ and $94.8X10^9$ particles, respectively.

4.1 Pressure

The pressure transducer was connected to the bed with a 7.3-cm long tube 5-mm inner diameter (Figure 4.1). The measuring port had a small portion of the mesh used at the bottom and top of the bed to prevent the particles from entering the tube.

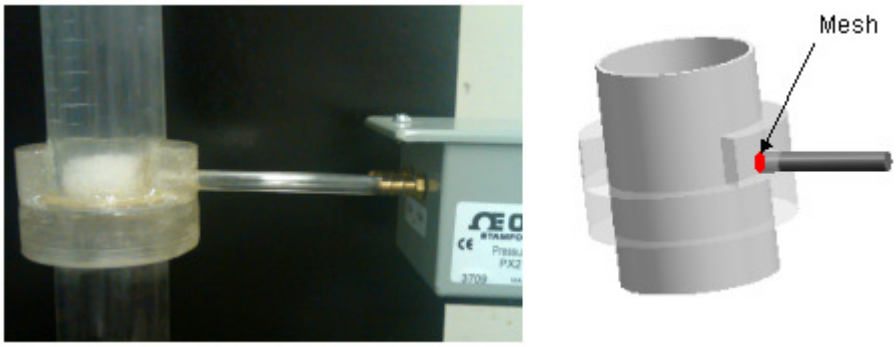

Figure 4.1: Pressure Measurement Port.

The first step in the experimental phase of the research was to determine the pressure and flow rates at which minimum fluidization and terminal velocities occur. This was achieved by first gradually increasing the air flow rate from zero to where particle separation starts at minimum fluidization velocity. Subsequently, the flow rate was increased using larger increments until the particles are entrained with the fluid and carried out of the bed, or in this case trapped in the mesh at the top of the bed. At this point, terminal velocity is achieved and the bed behavior between these two velocities is known as full fluidization.

4.2 High Speed Camera

The particles behavior at the top of the bed was recorded with the high speed camera at the fluid terminal velocity. The top of the bed was estimated to be at the highest point attained by a considerable amount of particles just before they are carried away with the fluid. These videos were later edited to obtain pictures of the particle movement and be analyzed in MatPIV.

4.2.1 MatPIV

After two images from the videos were selected to be analyzed, the first step was to change the format. Although the images seem black and white, they are stored as color images with three matrices. Each one corresponds to the colors red, green and blue (RGB Image) (Figure 4.2). These matrices indicate how much of each color each pixel should be used. Since MatPIV only works with images with 2D matrices the images had to be converted into Intensity image (gray scale image). This format represents an image as a matrix where every element has a value corresponding to how bright/dark the pixel should be colored (Figure 4.3). There are two ways to represent the brightness of the pixel, but the one used here is called "UNIT 8." This class assigns an integer between 0 and 255 to represent the brightness of the pixel in which 0 corresponds to black and 255 to white [16]. The Matlab command used to perform this transformation was:

$$NewImage = rgb2gray('FILENAME.FMT') \quad \textbf{4.1}$$

The text string FMT specifies the format of the file by its standard file extension.

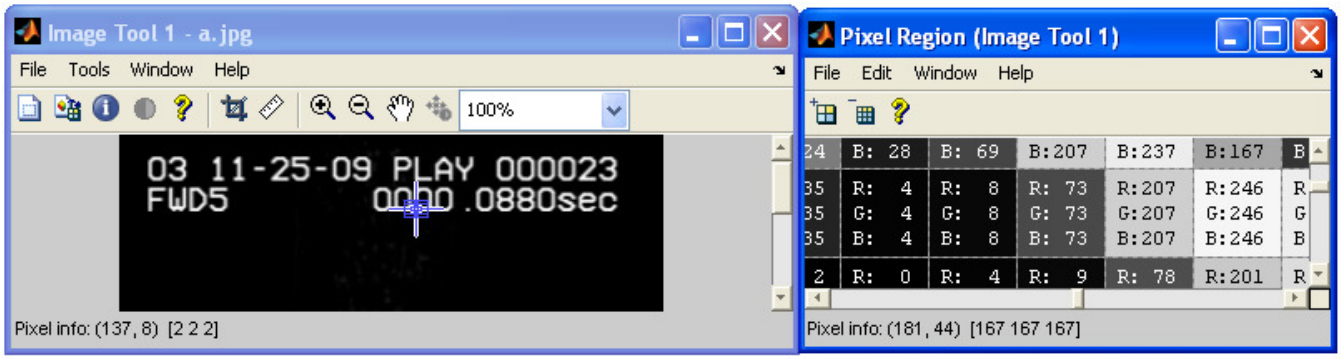

Figure 4.2: RGB Image Illustrating a Pixel Region.

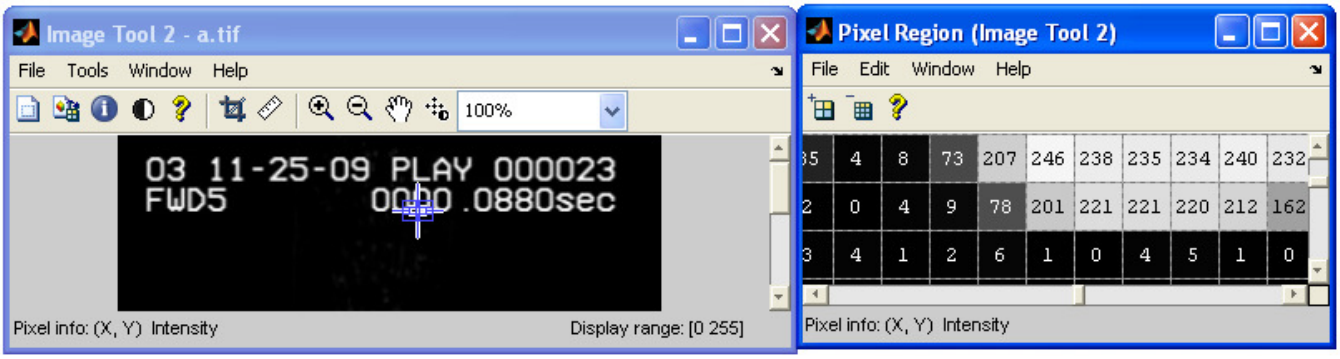

Figure 4.3: Gray Scale Image Illustrating a Pixel Region.

The next step in the image processing stage was to change the contrast of the images in order to detect the particles with the software. Figures 4.3 and 4.4 show the same image before and after being formatted.

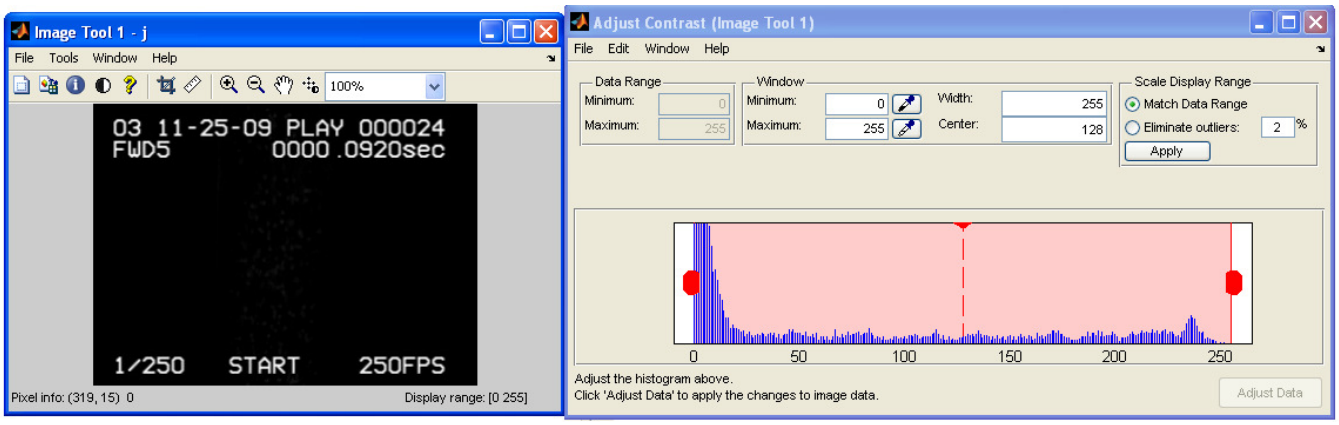

Figure 4.4: Gray Scale Image with Initial Contrast.

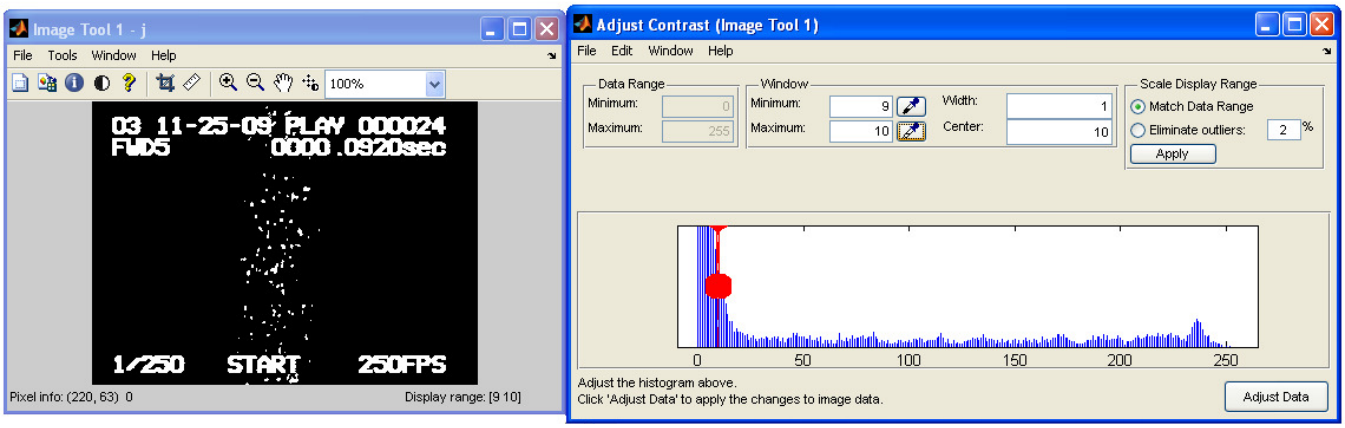

Figure 4.5: Gray Scale Image with Final Contrast.

The previous two processes (format and contrast change) were applied to every image. The Matlab commands used to carry out the analysis were obtained from [11]. One last element that is important to mention is the base image used to define the coordinate system and to determine how large each pixel is in the images. Figure 4.6, which was also changed in format and contrast, shows a grid with points that are 1 cm apart used in the MatPIV calculations. A different image, depending on the position and settings of the camera, was used for each bed.

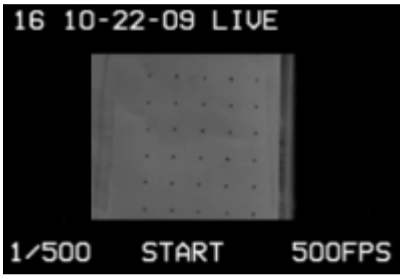

Figure 4.6: Image to Define Coordinate System.

4.3 Laser Doppler Anemometer

The same flow rates where terminal velocities were detected are used for the LDA measurements. The measuring point where the laser beams intersect was positioned with the aid of the high speed camera to place it at the center of the images taken with the camera. This point was also at the center of the bed and perpendicular to the surface (Figure 4.7) to avoid refraction of the laser light as mentioned in section 3.3.3.

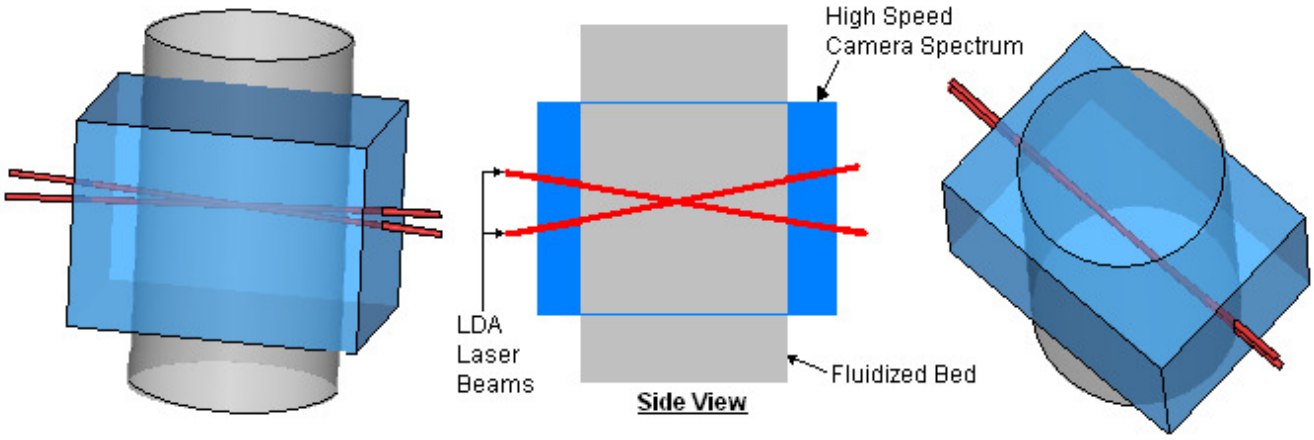

Figure 4.7: Highs Speed Camera and LDA Measurement Spectrums.

Chapter 5: RESULTS AND DISCUSSIONS

5.1 Pressure

Several pressure measurements were required to determine minimum fluidization and terminal velocities for all beds. Moreover, since the mass flowmeter would read volumetric flow rate (L/min) this had to be converted into gas superficial velocity (ft/s) with Equation 2.8 and other simple algebraic manipulations. These results are shown in Table 5.1.

Table 5.1: Minimum Fluidization and Terminal Velocities for All Beds.

Bed	Minimum Fluidization Velocity (ft/s)	Terminal Velocity (ft/s)
1 cm	0.69	16.92
3 cm	0.83	16.15
5cm	0.96	14.49

The DAQ assistant from LabVIEW was set to obtain 100 voltage readings per second. Since each flow rate was maintained for 20 seconds, about 108,667 readings were acquired in total for each bed. The average at each flow rate was used to plot differential pressure versus gas superficial velocity as shown in upcoming figures. Lastly, the pressure transducer had to be calibrated accordingly to the initial settings and the values attained at zero and maximum pressure. Those values were plotted (Figure 5.1), and the equation for the linear trend was used for the volts-psi relation.

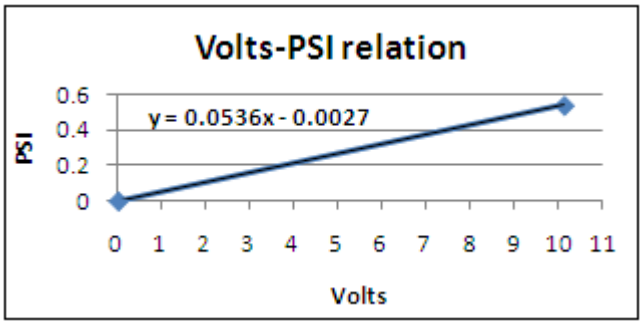

Figure 5.1: Pressure Transducer Calibration.

The results for minimum fluidization and terminal velocities at different gas superficial velocities for all beds are shown in Figure 5.2, 5.3, and 5.4, and Figure 5.5 compares the results from the three different particle concentrations. The graphs also show the small "hump" mentioned in Section 2.3 that was caused by the interlocking of the particles. This effect is less remarkable in the 5 cm bed because as the solid concentration increases there is more particle vibration at the bottom of the bed reducing the obstruction to the flow. As a result, this decreases the pressure spike before fluidization.

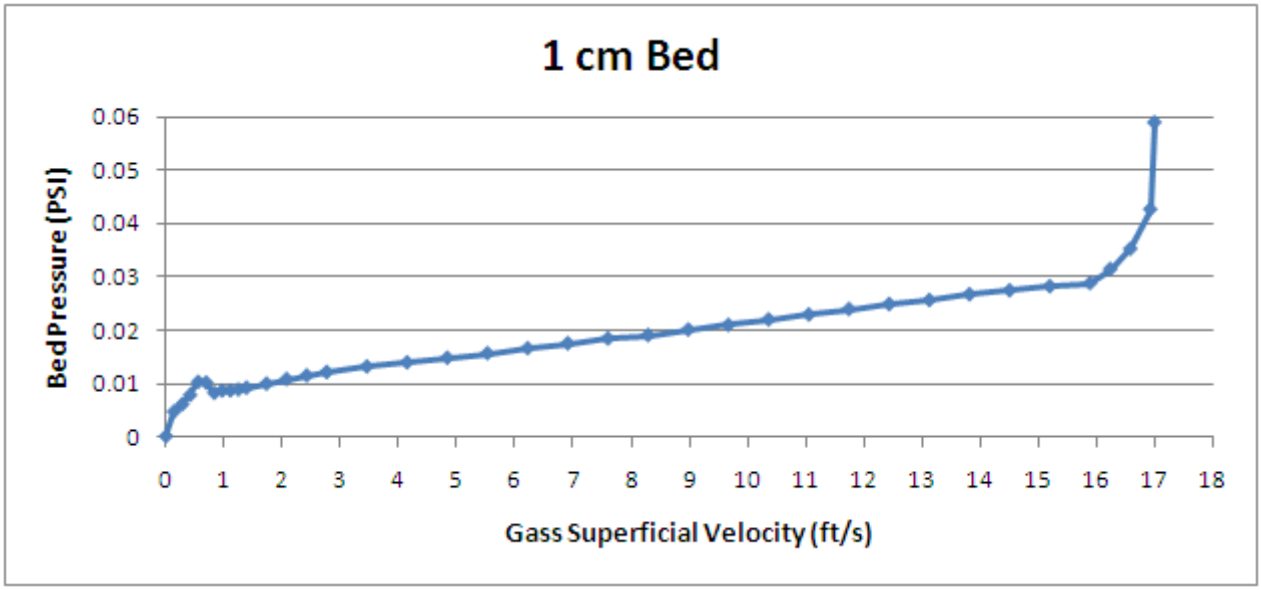

Figure 5.2: 1 cm Bed Pressure Behavior at Different Superficial Velocities.

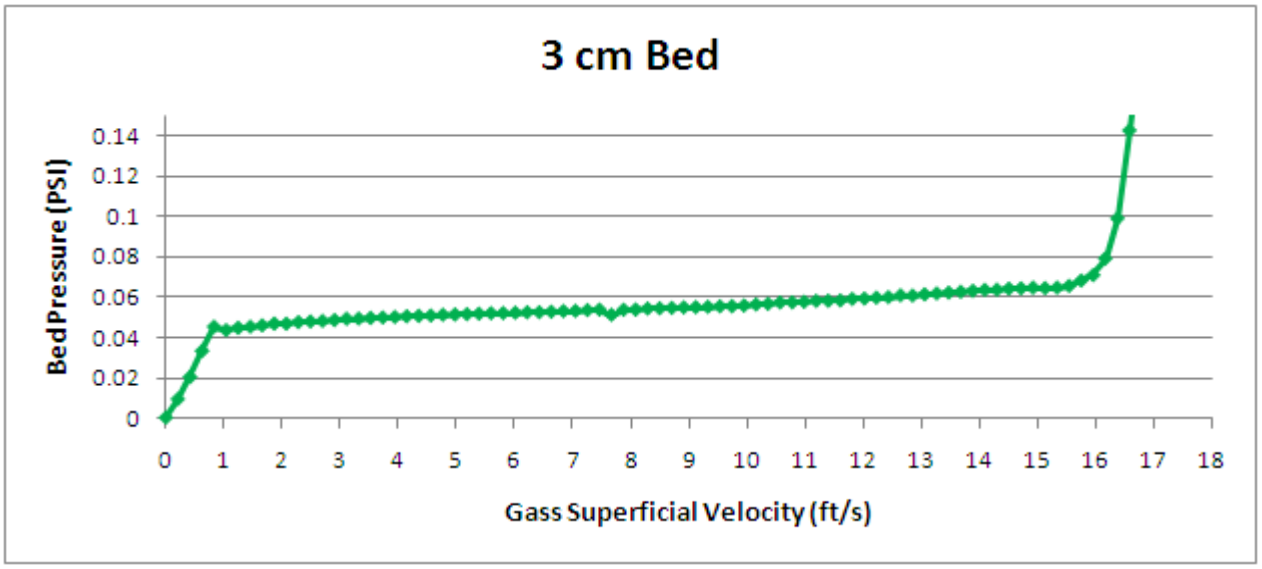

Figure 5.3: 3 cm Bed Pressure Behavior at Different Superficial Velocities.

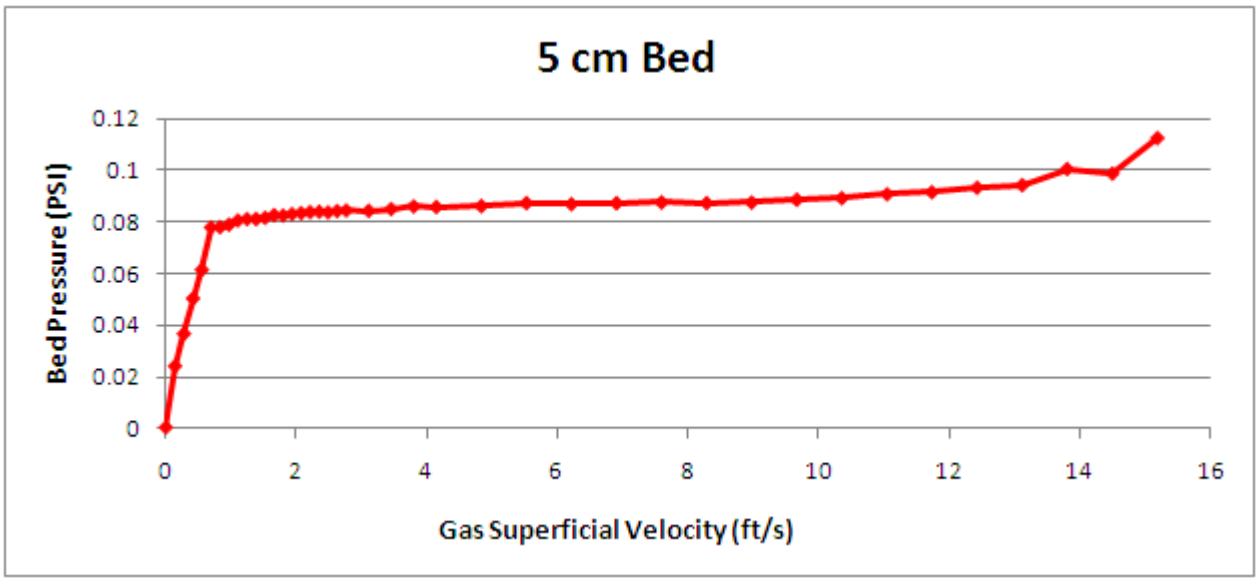

Figure 5.4: 5 cm Bed Pressure Behavior at Different Superficial Velocities.

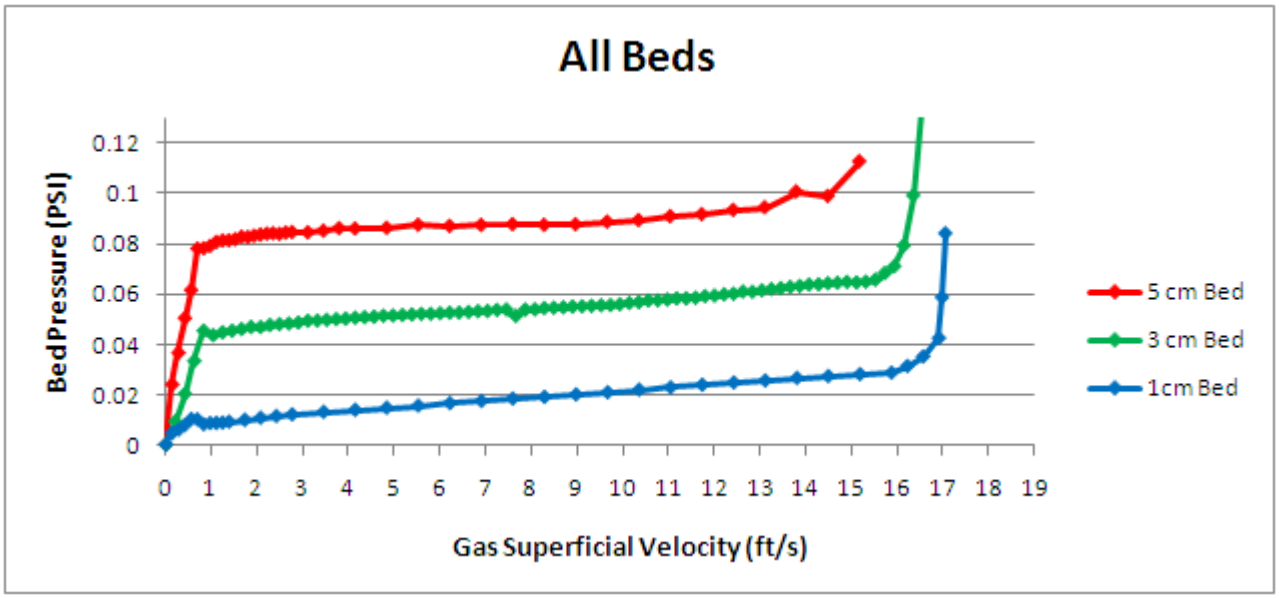

Figure 5.5: All Beds Bed Pressure Behavior at Different Superficial Velocities.

The pressure measurements shown above at minimum fluidization velocities can be corroborated with Equation 2.2.

$$\Delta_{\rho B} = \frac{Mg}{A} \qquad \textbf{2.2}$$

Gravity (g) and Area (A) are constants in the equation and the Mass (M) of the three different particle concentrations was discussed previously in Chapter 4. The pressure calculations for the three beds along with a multiplier to convert Pascals (Pa) into pounds per square inch (PSI) are shown below.

1 cm Bed

$$\boldsymbol{\Delta_{\rho B}} = \frac{0.01109\,\boldsymbol{X}\,9.81}{\pi\,\boldsymbol{X}\,(.016)^2} = 135.3\,Pa\,\boldsymbol{X}\,1.4508\,\boldsymbol{X}\,10^{-4} = \boldsymbol{0.0196\,PSI}$$

3 cm Bed

$$\boldsymbol{\Delta_{\rho B}} = \frac{0.03328\,\boldsymbol{X}\,9.81}{\pi\,\boldsymbol{X}\,(.016)^2} = 40.5.9\,Pa\,\boldsymbol{X}\,1.4508\,\boldsymbol{X}\,10^{-4} = \boldsymbol{0.0589\,PSI}$$

5 cm Bed

$$\boldsymbol{\Delta_{\rho B}} = \frac{0.05546\,\boldsymbol{X}\,9.81}{\pi\,\boldsymbol{X}\,(.016)^2} = 676.5\,Pa\,\boldsymbol{X}\,1.4508\,\boldsymbol{X}\,10^{-4} = \boldsymbol{0.0981\,PSI}$$

When comparing theoretical with experimental values in Table 5.2 the 1-cm bed has a more significant pressure difference against the other beds. The primary experimental error that may affect all the beds is the mesh in front of the tube mentioned in Section 4.1. Another significant affect primarily on the 1-cm bed is that the measuring port is almost as high as the concentration of particles. Ideally, this measuring point should be as small as possible compared to the height of the bed. For this reason the difference between theoretical and experimental values is less as the particle concentration increases.

Table 5.2: Experimental vs Theoretical Pressure Values.

Bed	Experimental	Theoretical	PSI Difference	% Difference
1 cm	0.0102	0.0196	0.0095	48.2
3 cm	0.0452	0.0589	0.0137	23.2
5 cm	0.0789	0.0981	0.0192	19.6

5.2 MatPIV Velocities

After obtaining the videos from the high speed camera, the videos were edited so images with different time intervals can be analyzed in MatPIV. Several images were tested and at the end two were selected from each particle concentration to perform the velocity analysis. Figure 5.6 shows an example of two pictures obtained from the fluidized bed with a 0.04-second interval. Since the particles are moving in a 3D plane, their movement is sometimes difficult to trace, which explains why MatPIV replaces the missing vectors using a nearest neighbor interpolation.

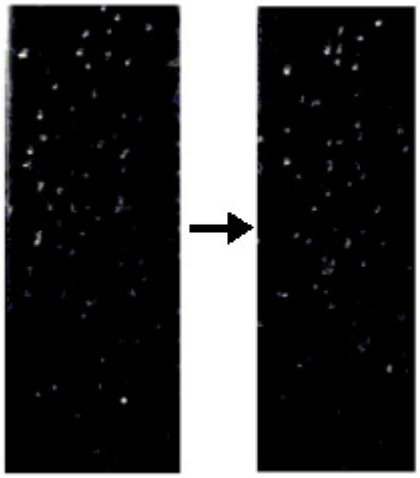

Figure 5.6: Fluidized Bed Images with 0.04 Seconds Interval.

Figures 5.7 through 5.12 show the filtered and interpolated velocity-field as well as the magnitude of the velocity for the three beds.

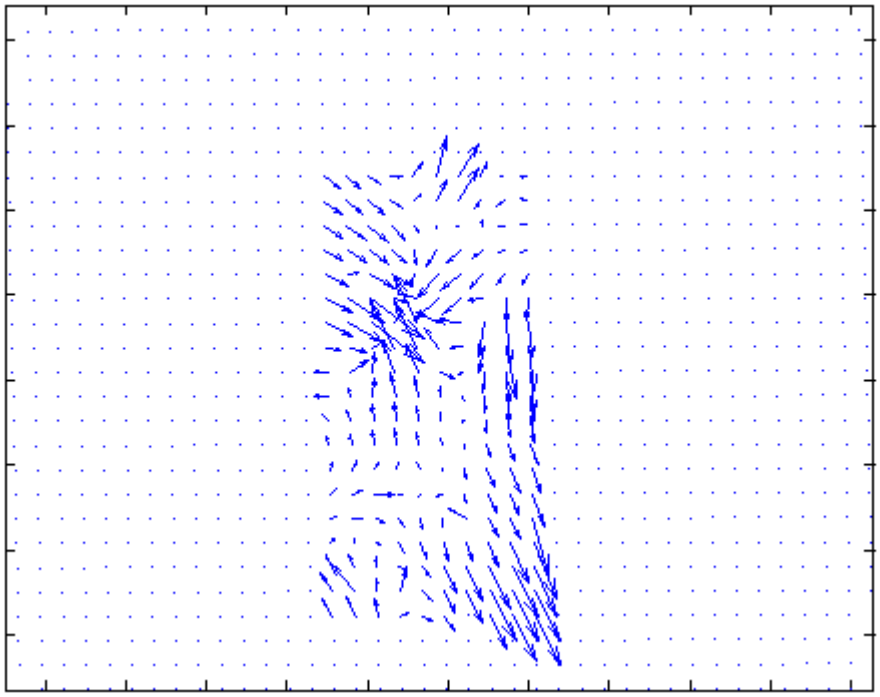

Figure 5.7: 1 cm Bed Velocity Vectors.

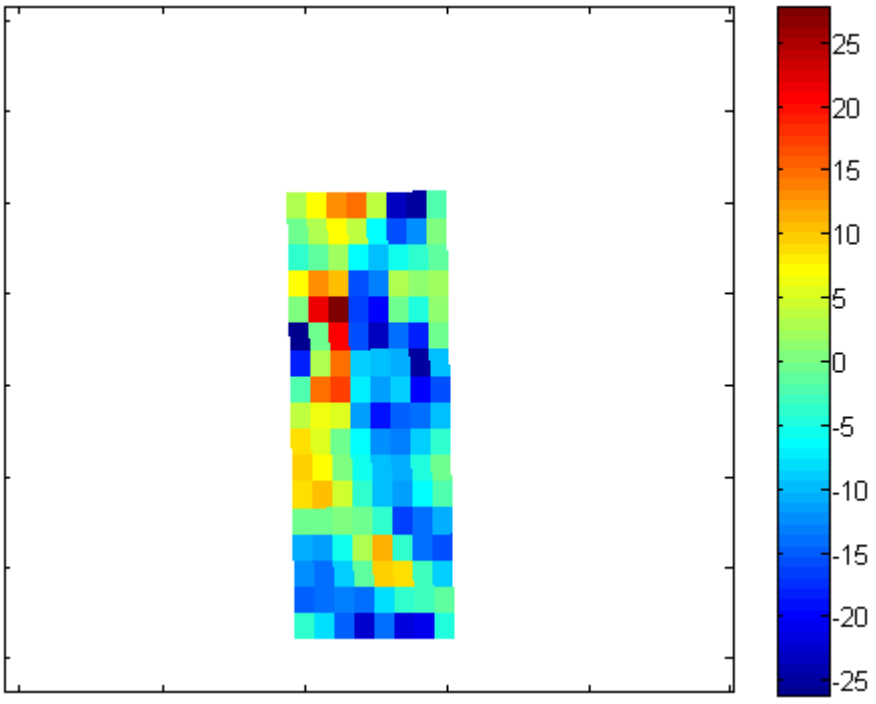

Figure 5.8: 1-cm Bed Magnitude of Velocity Vectors (Units: cm/s).

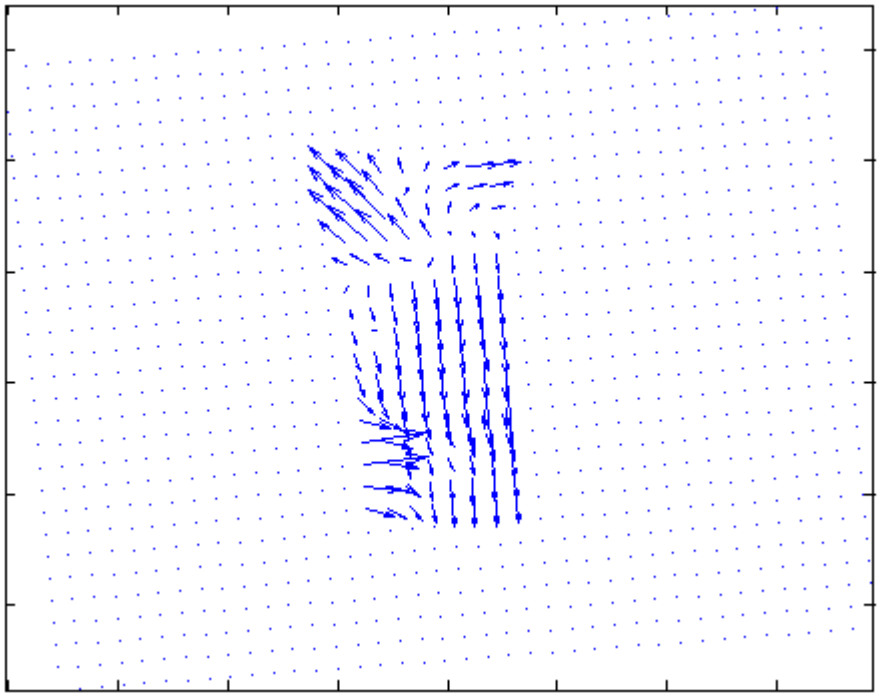

Figure 5.9: 3 cm Bed Velocity Vectors.

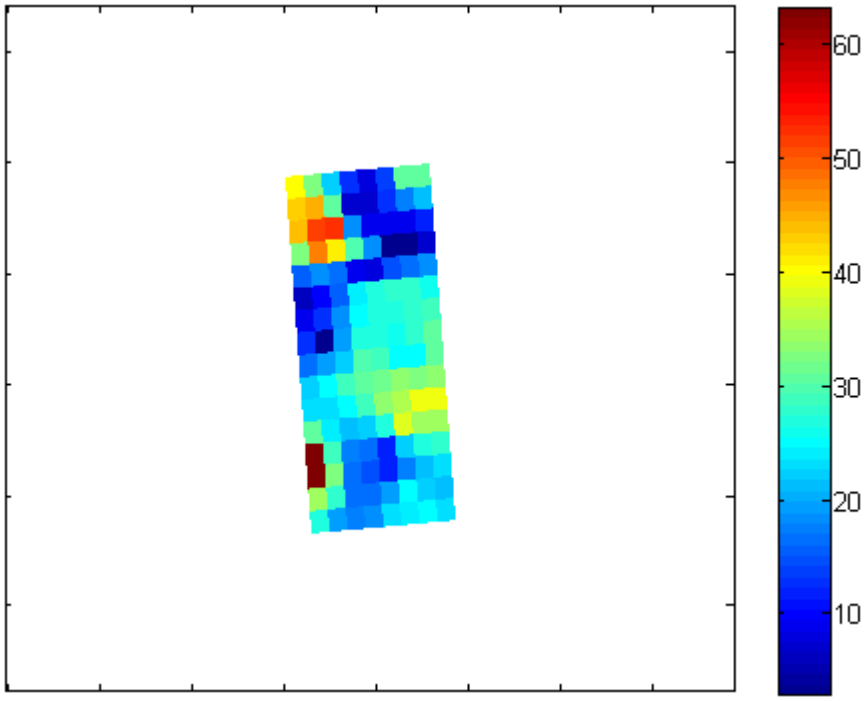

Figure 5.10: 3 cm Bed Magnitude of Velocity Vectors (Units: cm/s).

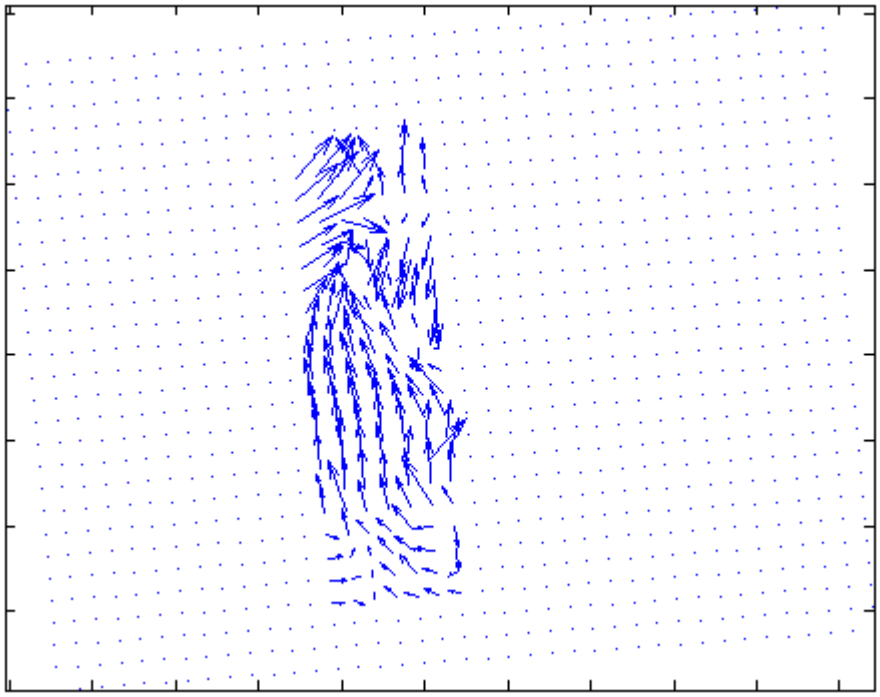

Figure 5.11: 5 cm Bed Velocity Vectors.

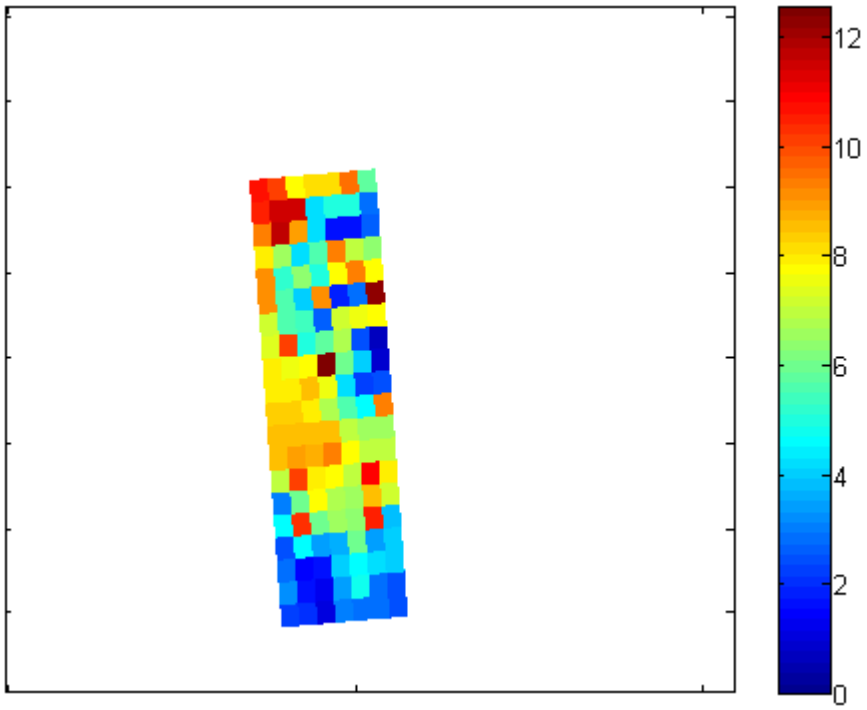

Figure 5.12: 5 cm Bed Magnitude of Velocity Vectors (Units: cm/s).

5.3 Laser Doppler Anemometer Velocities

After positioning the LDA probe where the laser beams intersect at the center of the bed, several measurements were attained. In order to obtain more accurate results and to corroborate the data, ten measurement tests were executed for each bed. As expected, more particle movement was detected with the LDA in the 5-cm bed as compared to the 1-cm bed. At each run, different particle readings were acquired, and the average is shown in Table 5.2.

Table 5.3: Average Particle Readings after 10 LDA Measurement Tests.

Beds	Average Readings
1 cm	47.1
3 cm	163.6
5 cm	231.5

Figures 5.13, 5.14 and 5.15 show the histograms for the measurements recurrence at different particle velocities for the 1-cm, 3-cm and 5-cm bed, respectively. The graphs also illustrate at what air flow rates along with the corresponding superficial velocities (U_s) the measurements were acquired. Moreover, the height at which the laser beams intersected the target area measured from the bottom of the bed is also included. The negative and positive velocities acquired by the LDA are particles moving opposite and parallel to the flow, respectively. The average negative velocities for the three beds only indicate that more particles crossed the intersecting beams in the opposite direction of the flow. Table 5.4 shows the average positive and negative velocities for the three beds.

Table 5.4: Average Negative and Positive Velocities for 1-cm, 3-cm and 5-cm Beds

Average	1 cm	3 cm	5 cm
Negative Velocities (ft/s)	-1.02	-1.05	-1.08
Positive Velocities (ft/s)	0.637	0.792	0.687

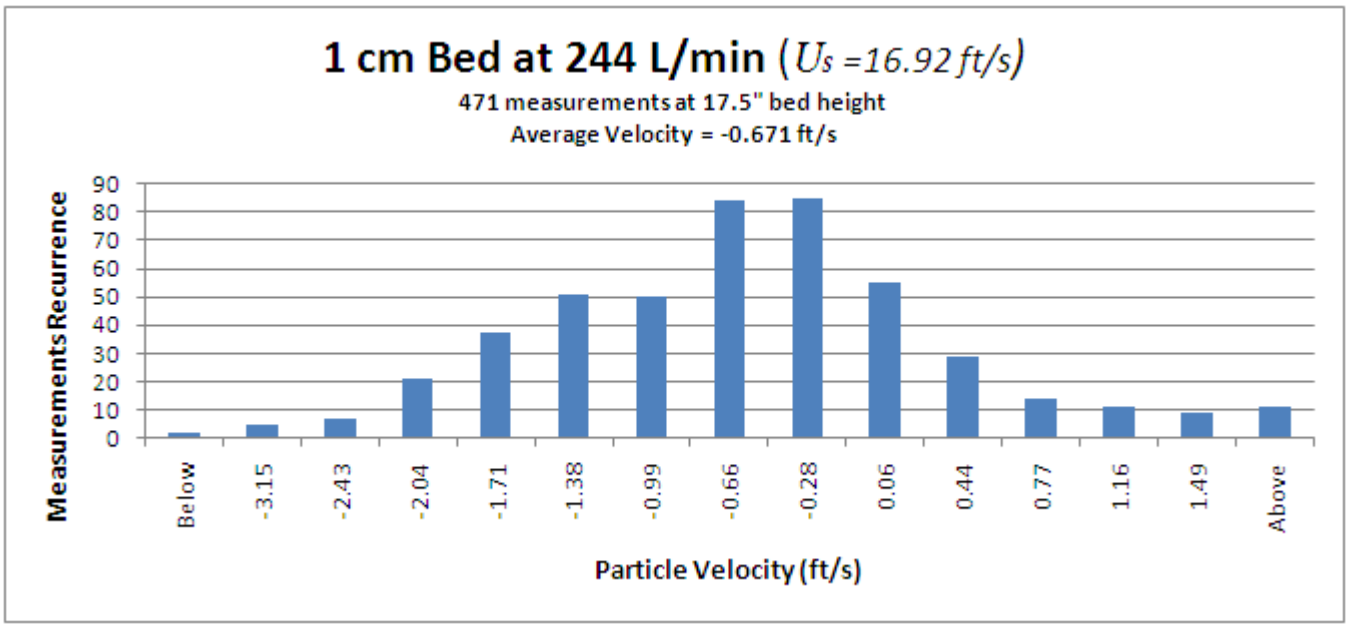

Figure 5.13: 1-cm Bed Measurements Recurrence at Different Particle Velocities.

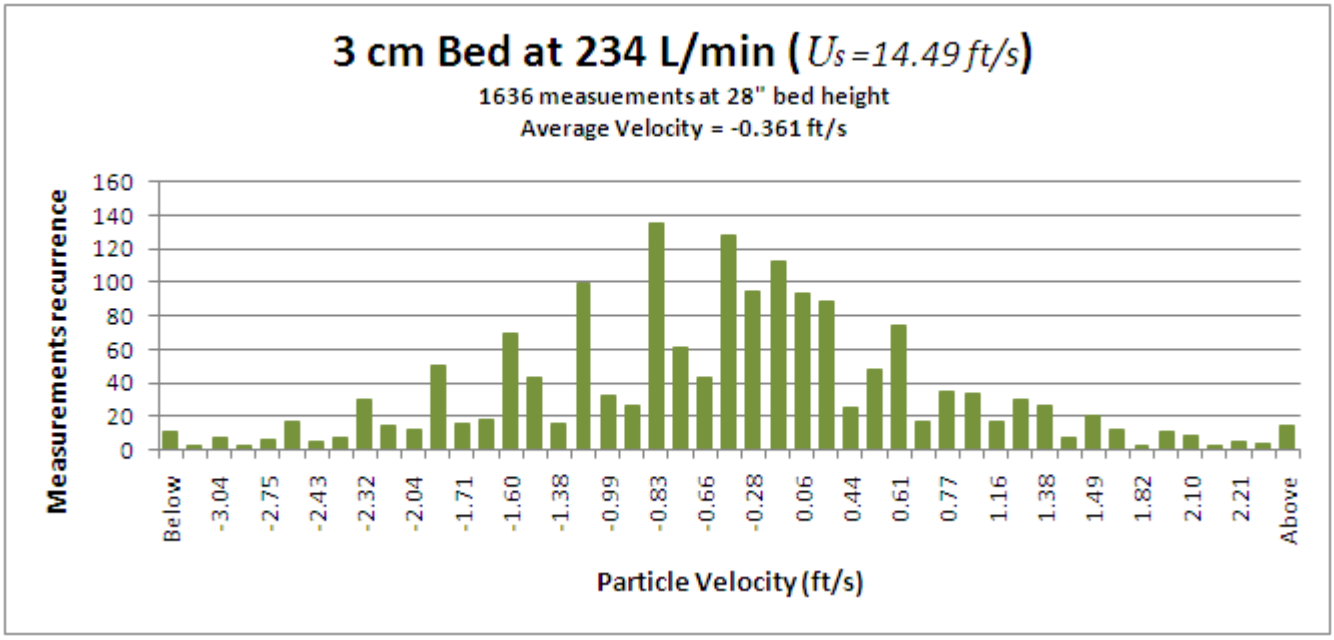

Figure 5.14: 3-cm Bed Measurements Recurrence at Different Particle Velocities.

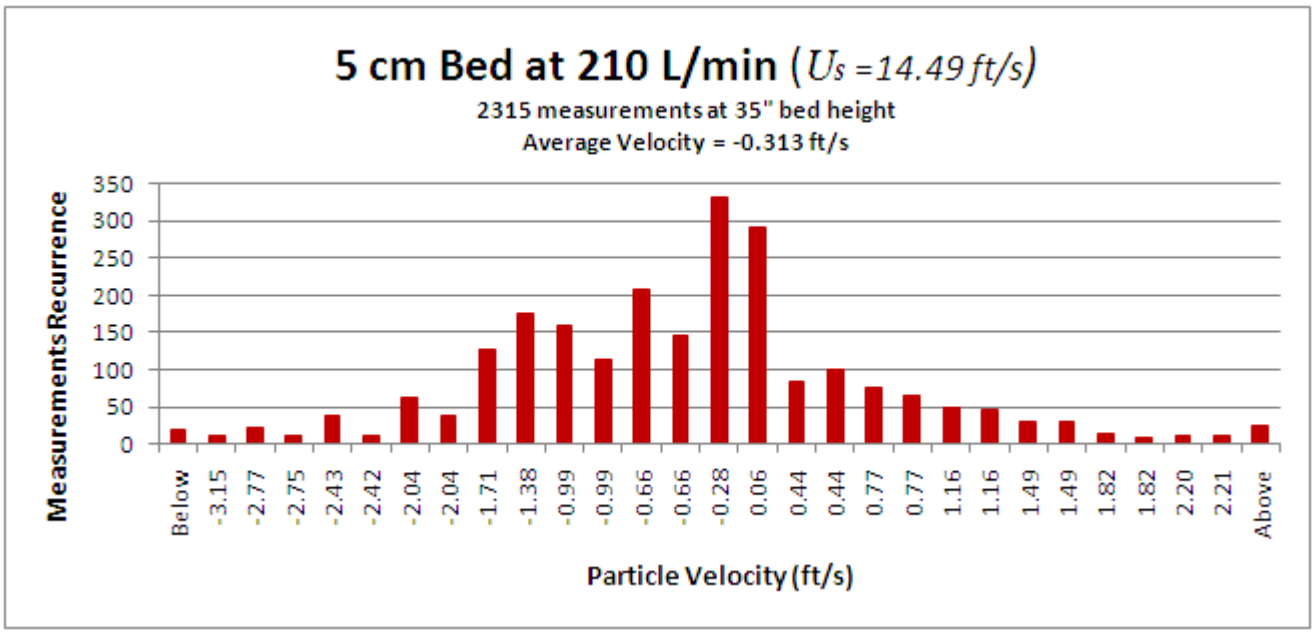

Figure 5.15: 5-cm Bed Measurements Recurrence at Different Particle Velocities.

5.4 Particles Behavior

Figure 5.16 shows how the particles behave for the 3-cm bed at minimum fluidization velocity. At this flow rate, particle separation occurs showing a bubbling behavior. Images (1) through (8) have an average time difference of 0.024 seconds.

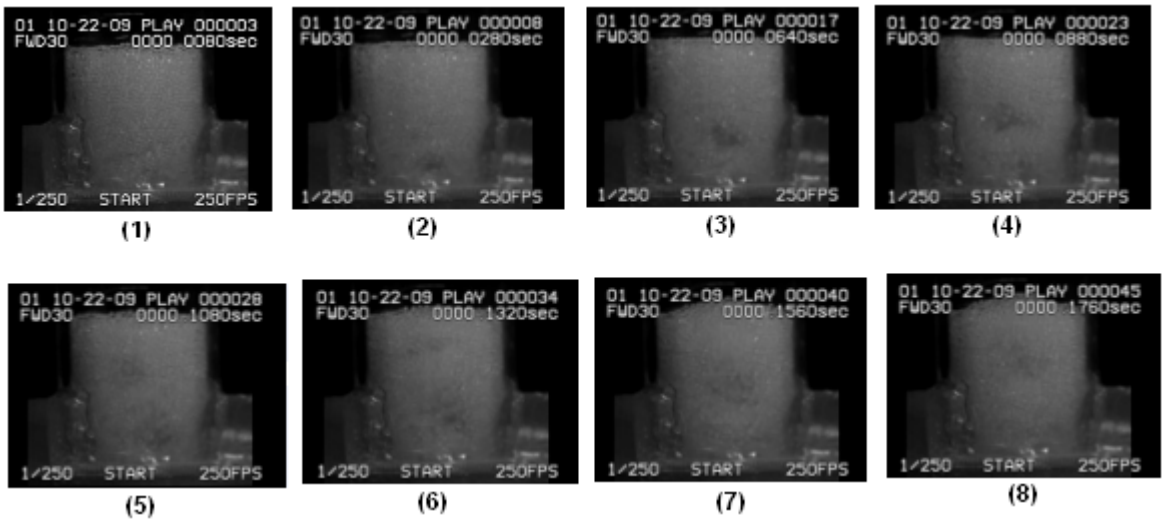

Figure 5.16: 3-cm Bed at Minimum Fluidization Velocity.

Figure 5.17 shows the fluidized bed behavior for the 5-cm particle concentration from 0 flow rate to just above terminal velocity.

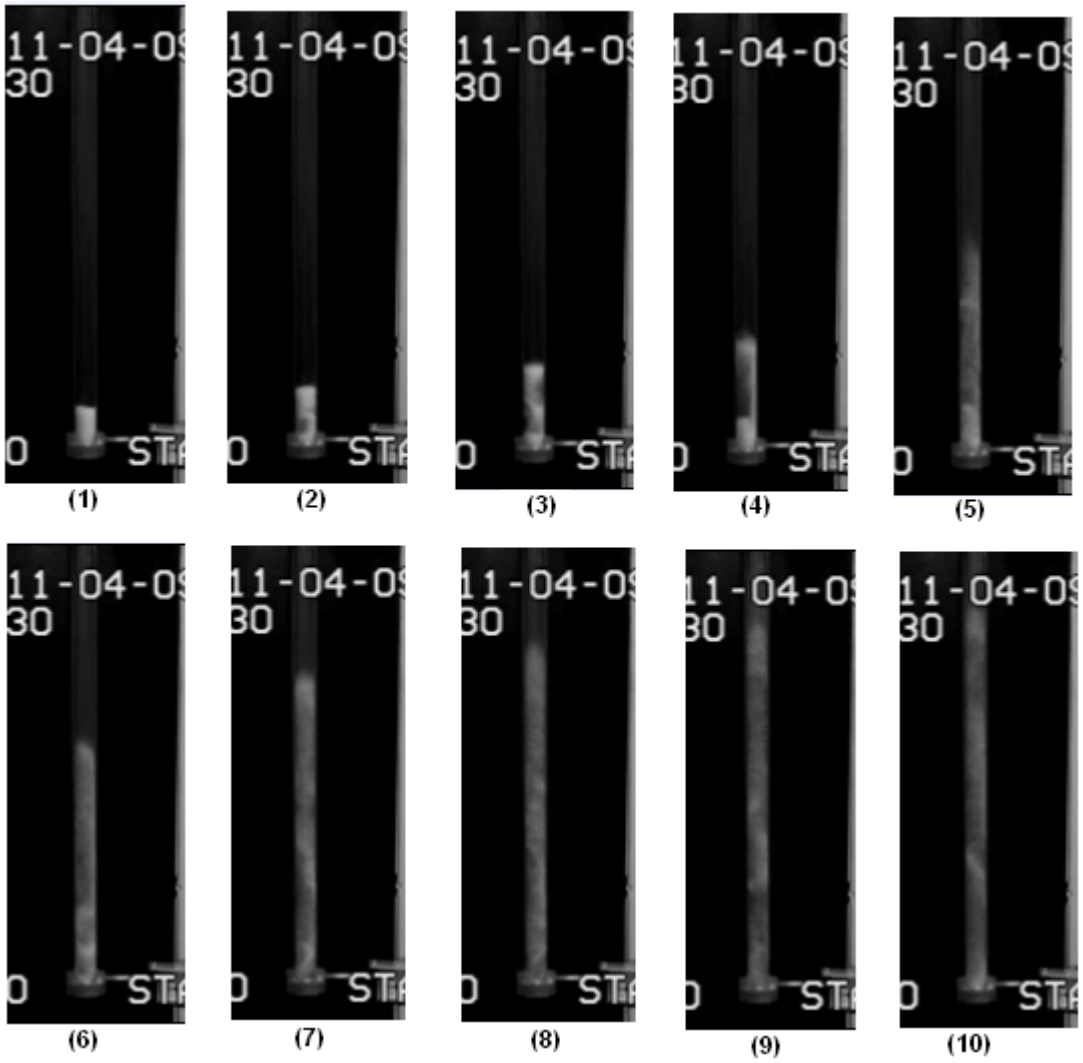

Figure 5.17: 5-cm Bed Behavior from 0 to Beyond Terminal Velocity.

Chapter 6: CONCLUSION AND RECOMMENDATIONS

6.1 Conclusion

An experimental study of the hydrodynamics of multiphase flow in a fluidized bed was covered in this paper. This investigation aims to contribute to future research in clean coal technology by explaining the fundamentals of a gasifier in coal gasification processes. A fluidized bed was designed and constructed to observe the behavior of three different particle concentrations at different air flow rates. Particle velocities were acquired with an LDA and MatPIV software. A differential pressure transducer was used to measure the change in pressure at the bottom of the bed.

The acquired graphs for pressure drop vs gas superficial velocity show a similar behavior to that covered in the literature review. Minimum fluidization and terminal fluid velocities were obtained as well as their corresponding pressure values. These were corroborated with theoretical calculations and a more significant difference was found in the 1-cm bed mainly because of experimental errors. Moreover, the histograms acquired with the LDA show more particle measurements as the solid concentration increases, proving to be a reliable data acquisition instrument. The attained negative average velocities for the three beds only indicate that more particles were measured in the opposite direction of the flow. The velocities in general provide a good understanding of how the particles behave at the top of the bed during fluid terminal velocity. At this point, images were obtained with the high speed camera to also measure particle velocity with MatPIV software. These results in contrast with those from the LDA measured the velocity of particles as a whole. Velocity vectors as well as the magnitude of their velocities were calculated for the three beds and were shown in images to understand particle distribution at the top of the bed. Video sequences from the high speed camera were also included to illustrate how the fluid-solid mixture expands across the bed at different flow rates. The project generated a wide and reliable database of the hydrodynamics in a fluidized bed, which will aid in the development of gasifiers for coal gasification processes.

6.2 Recommendations for Future Research

In the current study the only variable was particle concentration. In future research bed diameter and particle size can be used as the varying elements. Moreover, multiple beds can be constructed in such a way that different particles sizes can be easily input and/or removed from the set-up to carry out experiments with different initial conditions. This will provide a wider understanding of the hydrodynamics of fluidized beds.

Images of the bed at different distances from the bottom and at different flow rates can also be included to provide another perspective of the particle behavior. One last recommendation is the use of smaller ports for the pressure measurements and to position these as close as possible to the bottom of the bed. Furthermore, more accurate pressure readings can be obtained if a material other than the mesh can be selected to prevent the particles from getting inside the pressure device.

References

[1] F. Ju, et al., "Experimental study of a commercial circulated fluidized bed coal gasifier," Fuel Process. Technology Journal. (2009), doi:10.1016/j.fuproc.2009.07.013

[2] "Gasification Technology R&D," U.S. Department of Energy. 08/17/2009. http://www.fossil.energy.gov/programs/powersystems/gasification/index.html

[3] J. R. Howard, Fluidized Bed Technology: principles and applications, Adam Hilger; Adam Hilger, Bristol and New York, J R Howard 1989.

[4] Bruhns S., Werther J., "An Investigation of the Mechanism of Liquid Injection into Fluidized Beds", Particle Technology and Fluidization, AIChE Journal, March 2005, Vol 51, No. 3.

[5] Davidson J.F., Harrison D., FLUIDIZATION, Academic Press Inc 1971, Department of Chemical Engineering University of Cambridge, England.

[6] Subramanian, Shankar R., "Flow through Packed Beds and Fluidized Beds" summary obtained from: W.E. McCabe, J.C. Smith, and P.Harriott 2001. Unit Operations of Chemical Engineering, McGraw Hill, New York, *and* Perry's Chemical Engineers Handbook, 7th Edition. 1997 (Ed: R.H. Perry, D.W. Green, and J.O. Maloney), McGraw-Hill, New York.

[7] W.E. McCabe, J.C. Smith, and P.Harriott 2001. Unit Operations of Chemical Engineering, McGraw Hill, New York.

[8] **"**Anaerobic downflow stationary fixed-film treatment (III) Anaerobic expanded/fluidized bed treatment (V) Comparison of high-rate anaerobic wastewater treatment reactors (VI)", http://www.bvsde.paho.org/bvsair/e/repindex/repi54/anadow/anadow.html

[9] "SOLIDS NOTES 5, George G. Chase, The University of Akron", http://chemical.uakron.edu/fclty/chase/Solids/SolidsNotes5%20Fluidization.pdf

[10] Basu Prabir, Combustion and gasification in fluidized beds, CRC Press, 2006, Taylor and Francis Group.

[11] Sveen Kristian J., "An Introduction to MatPIV v. 1.6.1", Dept. of Math, University of Oslo, Mechanics and Applied Mathematics, No.2, ISSN 0809-4403, August 2004.

[12] Crowe, C., Sommerfeld, M., Tsuji, Y., 1998. Multiphase Flows with Droplets and Particles. CRC Press, Boca Raton, FL.

[13] Ibsen, C.H., Solberg, T., Hjertager, B.H., Johnsson, F., 2002. Laser Doppler anemometry measurements in a circulating fluidized bed of metal particles. Experimental Thermal and Fluid Science 26, 851–859.

[14] Taylor Jeffrey A., “Optical Measurement Techniques” ME637, Particle Transport Deposition and Removal II. http://74.125.47.132/search?q=cache:pHijw2n8uBAJ:web2.clarkson.edu/projects /crcd/me637/downloads/P_Jeff_lecture.pdf+how+the+dantec+lda+works%3F&cd=1&hl=en&ct=clnk&gl=us&client=firefox-a

[15] Dantec Measurement Technology Denmark, “BSA/FVA Flow Software”, Installation & User’s guide, Vol 1. Fourth Edition, Printed in 2000.

[16] Kristian Sandberg., "Introduction to Image Processing In Matlab1”, Department of Applied Mathematics, University of Colorado at Boulder. http://amath.colorado.edu/courses/5720/2000Spr/Labs/Worksheets/Matlab_tutorial/matlabimpr.html

Appendix

Components Specifications

Table 1: SMC AC40-N04C3-Z Air Filter, Pressure Regulator & Lubricator.

Description	Specifications
Fluid	Air
Max. operating pressure	1.0 Mpa
Set Pressure Range	0.05 to 0.85 Mpa
Ambient and Fluid temperature	-5 to 60°C (with no freezing)
Bolw Material	Polycarbonate
Weight (kg)	1.74

Table 2: INGERSOLL-RA ND SSR-EP25 Air Compressor.

Description	Specifications
Capacity	97 CFM
Max Discharge Pressure	125 PSIG
Nominal Drive Motor	25 H.P.
Total Package Amps	64/32
Volts	230/460
Phase/Herts	3/60
Control Voltage	120

Table 3: Omega FMA 1845 Digital Mass Flowmeter.

Description	Specifications
Units	SLM
Range	0-1000 L/min
Type	Linear
Output	0 to 5 Vdc
Maximum Pressure	500 PSIG
Operating Voltage	12 Vdc
Accuracy	±1.5% of full scale

Table 4: PHOTRON FASTCAM-Super 10K High Speed Camera.

Description	Specifications
Image sensor	CCD
Features	High speed recording up to 1000 frames/sec
Recording media	IC memory (DRAM), 128 Mbytes
Recording rate	Full frame-512x480 pix and 30;60;125;250 FPS
Recording capacity	546 full frames
Shutter speed	1/recording rate; 1/500 to 1/20,000 sec.

Table 5: LOKO-Power Supply DPS-3050.

Description	Specifications
Input Voltage	115VAC ± 10%
Output Voltage	0 ~ 50VDC (Adjustable)
Output Current	0~3A (Adjustable)

Table 6: Omega PX277-30D5V Differential Pressure Transducer.

Description	Specifications
Excitation	12 to 35 Vdc
Output	0 to 5 or 0 to 10 Vdc selectable
Accuracy	±1% FS
Operating temperature	0 to 175°F
Pressure fittings	0.2" hose barbs
Pressure selectable ranges (inH2O)	0 to 30, 0 to 15, 0 to 7.5, -15 to 15, -7.5 to 7.5, -3.75 to 3.75

Table 7: OHAUS AV53 Adventurer Pro Precision Balance.

Description	Specifications
Capacity	51 g
Readability	0.001 g
Repeatability (std. dev)	0.001 g
Linearity	± 0.002
Stabilization	2.5 seconds

Table 8: Swagelok SS-1RS8 Needle Valve for Precise Flow Control.

Description	Specifications
Flow Pattern	Straight (2-way)
Valve material	Stainless Steel
End connections size	1/2 in
End connections type	Swagelok® tube fitting
Handle style	Phenolic knob
Max Temperature with Pressure Rating	450°F @ 3435 PSIG / 232°C @ 236 BAR
Orifice	250 in
Room Temperature Pressure Rating	5000 PSIG @ 100°F / 344 BAR @ 37°C

Vita

Gerardo Vargas Duarte was born on August 9, 1983 in Chihuahua, MEXICO. The eldest son of Gerardo de Jesus Vargas Guzman (R.I.P.) and Yolanda Guadalupe Duarte Lara, he graduated from "Preparatoria 20-30" high school in Delicias Chihuahua, MEXICO in 2002 and joined The University of Texas at El Paso (UTEP) in 2003 to pursue a Bachelor of Science in Mechanical Engineering. During this time he was a Teaching Assistant for Fluid Mechanics, Dynamic Response and Graphics in Engineering Design, conducting lessons of Unigraphics NX4. After completing the BS degree he began attendance for a Master of Science in Mechanical Engineering at UTEP. During his first semester as a graduate student, he attended a summer internship with Chrysler LLC in Auburn Hills, Michigan, in which he was part of the Product Development Group. His accomplishments include being part of Pi Tau Sigma, Tau Beta Pi, Mexican American Engineers and Scientists (MAES), Society of Hispanic Professional Engineers (SHPE) and acting as President and Treasurer for the Society of Automotive Engineers (SAE).

Permanent address: Ave. de la Esperanza # 301
Delicias Chihuahua, MEXICO, 33000

This thesis/dissertation was typed by Gerardo Vargas Duarte